Revue de micropaléontologie 84 (2024) 100789

Contents lists available at ScienceDirect

Revue de micropaléontologie

journal homepage: www.elsevier.com/locate/revmic

Miocene radiolarian assemblages from the submarine Vityaz Ridge, Northwest Pacific: Biostratigraphy and paleoceanography

Assemblages de radiolaires du Miocène de la ride sous-marine de Vityaz, Pacifique Nord-Ouest : Biostratigraphie et paléoocéanographie

L.N. Vasilenko[a,*], Yu.P. Vasilenko[a], Xuefa Shi[b], Yanguang Liu[b,c]

[a] *V. I. Il'ichev Pacific Oceanological Institute FEB RAS, Vladivostok 690041, Russian Federation*
[b] *Key Laboratory of Marine Geology and Metallogeny, First Institute of Oceanography, Ministry of Natural Resources, Qingdao 266061, China*
[c] *College of Ocean Science and Engineering, Shandong University of Science and Technology, Qingdao 266590, China*

ARTICLE INFO

Keywords:
Radiolarian assemblages
Biostratigraphy
Miocene
Submarine Vityaz Ridge
Kuril–Kamchatka Trench

Mots-clés:
Assemblages de radiolaires
Biostratigraphie
Miocène
Ride sous-marine de Vityaz
Fosse Kouriles-Kamchatka

ABSTRACT

This study presents the first data on radiolarian fauna from Miocene deposits of the submarine Vityaz Ridge (SVR) and paraxial zone of the Kuril-Kamchatka Trench. Twenty-two dredge samples were studied, and 214 radiolarian taxa were identified. Taxonomic composition allowed their assignment to Miocene assemblage zones, including *Lipmanella japonica conica-Gondwanaria dogieli, Pentactinosphaera hokurikuensis, Dendrospyris sakaii, Eucyrtidium inflatum* Subzone a, *Lychnocanoma magnacornuta*, and *Lychnocanoma parallelipes* zones. These radiolarian assemblages correlate with studied sequences of many deep-sea cores in the northern Pacific and some sections of onshore Japan. As a result, we designed a biostratigraphic scheme of Miocene radiolarians for the SVR and reconstructed the environmental conditions in this area. In particular, two Miocene climatic optima that were previously established in the northern Pacific were identified in the Middle and Upper Miocene sediments of the southern plateau and Middle Miocene sediments of the northern plateau of the SVR.

Résumé: Cette étude présente les premières données sur la faune à radiolaires des dépôts miocènes de la ride sous-marine de Vityaz (SVR) et de la zone paraxiale de la fosse Kouriles-Kamtchatka. Vingt-deux échantillons ont été étudiés et 214 taxons de radiolaires ont été identifiés. La composition taxinomique a permis leur affectation aux zones d'assemblage du Miocène, notamment *Lipmanella japonica conica-Gondwanaria dogieli, Pentactinosphaera hokurikuensis, Dendrospyris sakaii, Eucyrtidium inflatum* Sous-zone a, *Lychnocanoma magnacornuta* et *Lychnocanoma parallelipes*. Ces assemblages de radiolaires sont corrélés avec les séquences de nombreuses carottes réalisées en eaux profondes dans le nord du Pacifique et dans certaines parties de la côte japonaise. En conséquence, nous avons conçu un schéma biostratigraphique des radiolaires du Miocène pour la SVR et reconstruit les conditions environnementales dans cette zone. En particulier, deux optima climatiques du Miocène précédemment établis dans le Pacifique Nord ont été identifiés dans les sédiments du Miocène moyen et supérieur du plateau sud et du Miocène moyen du plateau nord de la SVR.

1. Introduction

Active investigations of the geological structure of the Kuril-Kamchatka arc-trench system (KKS) began in the second half of the 20th century. For this purpose, a series of sea expeditions were carried out in this system (Udintsev, 1955; Vasiliev et al., 1979; Vasiliev, 1988; Kulinich et al., 2007; 2015) (Fig. 1), and dredge samples were collected. These samples have been studied extensively (Lelikov et al., 2008; Terekhov et al., 2012, 2013), and the age and composition of the rocks were determined. Age determinations were mainly performed by analyzing diatoms and silicoflagellates (e.g., Tsoy, 2002, 2011, 2014), while limited radiolarian analyses were performed. Based on radiolarians, an Eocene–Lower Miocene age was established for the dredge samples of the submarine Vityaz Ridge (SVR) (Tochilina, 1985; Vasilenko, 2017), Kuril Basin, and continental slope of eastern Kamchatka (Popova, 1989; Tsoy et al., 2000; Tsoy and Shastina, 2005). The radiolarian assemblages identified in the sediments of these areas were similar to those used to establish radiolarian biostratigraphic schemes based on material from West Siberian Paleogene formations (Kozlova and Gorbovets, 1966; Lipman et al., 1960), the Norwegian

* Corresponding author.
E-mail address: lidia@poi.dvo.ru (L.N. Vasilenko).

https://doi.org/10.1016/j.revmic.2024.100789
Received 12 September 2023; Received in revised form 18 March 2024; Accepted 3 May 2024

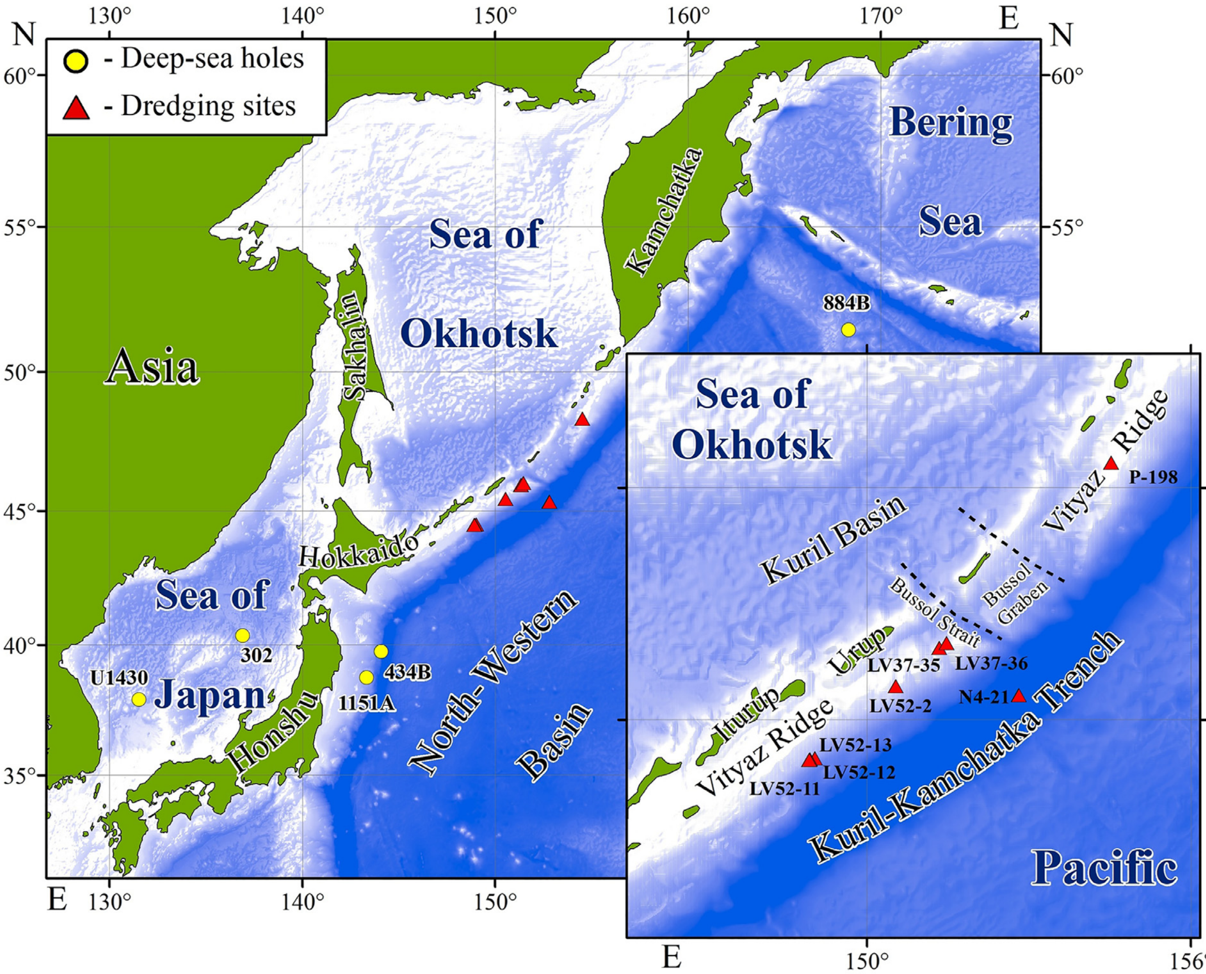

Fig. 1. Locations of the dredged samples (red triangles) and referenced scientific drilling sites (yellow circles). The dashed line indicates the Bussol graben (Kulinich et al., 2015).

Sea (Bjorklund, 1976; Strelkov and Petrushevskaya, 1979), marine sediments from the islands of Japan (Funayama, 1988), and the island slope of the Japan Trench (Motoyama, 1996; Tochilina, 1991, 2013). Although radiolarians of Middle Miocene age were not found in the dredge samples, those of Middle Miocene–Early Pliocene age were identified in the sections from Iturup and Kunashir islands (Great Kuril Ridge) (Runeva and Ushko, 1984; Vitukhin, 1989; Vitukhin et al., 1996). Studies revealed radiolarian zones in these sections that were previously established in the sections from the islands of Japan (Nakaseko and Sugano, 1973; Funayama, 1988) and Sakhalin Island (Runeva, 1981; Vitukhin, 1993). In dredge samples from the continental slope of eastern Kamchatka (Kronotsky Bay), only single specimens of radiolarians were found, including Late Miocene–Pleistocene species previously identified in the zonal assemblages of the Sea of Japan region (Tsoy et al., 2000). Pleistocene radiolarians were identified in the dredge samples from the SVR (Vasilenko and Vasilenko, 2021). The biostratigraphic sequence of radiolarian assemblages corresponds to the zoned assemblages recognized in the Northwest Pacific (Hays, 1970; Motoyama, 1996; Kamikuri et al., 2017).

In this study, we provide a detailed examination of the Miocene radiolarian assemblages in the sediments of the SVR. We analyzed 20 dredge samples from the SVR and 2 dredge samples from the paraxial zone of the Kuril-Kamchatka Trench (KKT) opposite the Bussol Strait. Our findings clarify and supplement the Miocene radiolarian biostratigraphic scheme for this region.

2. Study area

2.1. Geological and paleoceanographic setting

The KKS includes the active subduction zone and transition area between Northeast Asia and the Northwest Pacific. The Kuril Basin (Sea of Okhotsk), Kuril Island arc, and KKT are the main structures in the island arc-trench system (Sergeev, 1976; Fig. 1). The KKT extends for 2,200 km from the Tsugaru Strait in the south to the Kamchatka Strait in the north. The Kuril Island arc extends for 1,175 km (parallel to the KKT) from Hokkaido in the south to Kamchatka in the north and consists of the Greater (internal) and Lesser (external) Kuril Chains, which are separated by a trough (Khomich et al., 2019). The SVR is a trench-ward submarine continuation of the Lesser Kuril Chain and is divided into a southern and northern plateau by the Bussol graben (Vasiliev et al., 2001; Kulinich et al., 2007; 2015).

Cenozoic sediments are widespread throughout the Kuril Island arc and along the island slope of the KKT (e.g., Sergeev, 1976; Vasiliev et al., 2001). According to Vasiliev et al. (2001), the Cenozoic deposits of the Kuril Island arc and its Pacific slope consist of five stratigraphic units: Paleocene, Eocene–Lower Miocene, Middle Miocene, Upper Miocene–Lower Pliocene, and Upper Pliocene–Pleistocene. Subsequent studies established three lithostratigraphic units in the SVR: Paleocene–Eocene (?), Oligocene–Middle Miocene and Pliocene–Pleistocene (Kulinich et al., 2007; Lelikov et al., 2008; Terekhov et al., 2012, 2013). These researchers distinguished two marine stages of sedimentation in the geological evolution of the SVR: Paleocene–Middle Miocene and Pliocene–Pleistocene. Paleocene-Eocene (?) sediments do not contain microfossils. Based on diatom analysis, Oligocene–Early Miocene sediments (the first marine stage) were formed under shelf conditions. The exception is the sediments of the Bussol Strait and the southern SVR plateau, which formed under upper bathyal conditions (Terekhov et al., 2013). Middle Miocene sediments accumulated under upper bathyal conditions with the active input of nearby terrigenous material, Pliocene–Pleistocene sediments (second marine stage) accumulated under deep-sea bathyal conditions, while Middle Pleistocene sediments of the upper slope of the southern plateau of the SVR formed under shelf conditions. Based on radiolarian analysis, Vasilenko and Vasilenko (2021) established that a sedimentation hiatus from the Middle to beginning of the Late Pleistocene occurred in this area.

2.2. Climate in the Neogene

According to Gladenkov (1982, 1988), the Oligocene–Early Miocene was characterized by climate cooling in the North Pacific (e.g., Japan, Sakhalin, Kamchatka, and Alaska). At the end of the Early to beginning of the Middle Miocene, a noticeable warming occurred (the first climatic optimum), reflected in the presence of relatively warm-water species of fauna and flora. At the end of the Middle Miocene, after a period of cooling, a second climatic optimum occurred, which was also characterized by the presence of warm-water species. This optimum is assumed to be less significant than the first. At the end of Miocene–Pliocene, gradual climate cooling occurred. Runeva and Ushko (1984) identified warm-water radiolarian species in the Upper Miocene–Lower Pliocene sediments of Kunashir Island (Great Kuril Chain) that likely reflected a third, minor climatic optimum in the southern Kuril Islands, centered on the Early Pliocene.

2.3. Oceanography of the studied area

Modern conditions of the KKS system are determined by the influence of water masses of the Pacific Ocean and Bering, Okhotsk and Japan seas (Leonteva, 1985). The Kamchatka Current flows from the Bering Sea in the northwestern Pacific (Worne et al., 2019) and mixes with Pacific waters. Then, part of this current enters the Sea of Okhotsk through the straits between the northern Kuril Islands as the warm West Kamchatka Current, while the rest of the flow follows along the KKS to the south, in the form of the Oyashio Current. Accordingly, these water masses have a significant impact on the north of the KKS and its entire oceanward part. The Sea of Okhotsk waters mainly flow into the Pacific through the Bussol Strait and southern part of the Kruzenshtern Strait, with a minor flow occurring through the straits between the southern Kuril Islands as well (Leonteva, 1985). In the south, the KKS is influenced by the Sea of Japan waters. The warm Soya Current flows through the strait between Sakhalin Island and Hokkaido Island into the southwest of the Kuril Basin, where it mixes with the Sea of Okhotsk waters. This mixed water mass then flows out from the Sea of Okhotsk through the straits between the southern Kuril Islands. The Tsugaru Current flows out from the Japan Sea through the strait between Hokkaido and Honshu islands, mixes with the Kuroshio Current, and continues to the northeast. These water masses reach the south of the KKS in the form of mesoscale ocean eddies.

3. Materials and methods

In this study, we analyze the radiolarian fauna from SVR and KKT dredge samples and compare it to the assemblages used to develop biostratigraphic schemes for the adjacent portions of the northwest Pacific.

We then develop a radiolarian biostratigraphic scheme for our study region, correlate it to existing diatom and silicoflagellate zonations, and use it to recognize the evolution of the SVR in the Miocene.

3.1. Materials

In this study, 22 dredge samples were analyzed from the SVR and paraxial zone of the KKT (Table 1). These samples were collected during cruise 31 of the R/V *Pervenets* in 1978, cruise 4 of the R/V *Akademik Alexander Nesmeyanov* in 1984, and cruises 37 and 52 of

Table 1
Descriptions of the dredge samples and referenced scientific ocean drilling holes.

Sites	Locations	Depth, meters below sea level	ID Hole/ Dredge sample	Lithology	References
884	51°27.03´ N 168°20.23´ E	3824.8	884B	–	(Morley, Nigrini, 1995; Kamikuri et al., 2007)
1151	38°45´ N 143°20´ E	2182.2	1151A	–	(Kamikuri et al., 2004)
U1430	37°54.16´ N 131°32.25′ E	1072	U1430A, U1430B, U1430C	–	(Tada et al., 2015; Kamikuri et al., 2017)
N4-21	45°19.00´ N 152°49.00´ E	8640–8960	N4-21/2-1	diatomaceous clay with ash	this study
			N4-21/2-2	diatomaceous clay with ash	this study
P-198	48°19,2´ N 154°31,7´ E	350–240	P-198-5	tuff siltstone	this study
			P-198-14	tuff siltstone	this study
			P-198-19	tuff siltstone	this study
LV37-35	45°55.880´ N 151°20.514´ E	1760–1650	LV37-35-1	tuff siltstone with tuff sandstone lens	this study
LV37-36	45º59.9´ N 151º29.0´ E	2100–1800	LV37-36-1	clayey tuff siltstone	this study
			LV37-36-3	mudstone	this study
			LV37-36-5	tuff siltstone	this study
LV52-2	45°25.935´ N 150°32.466´ E	600–560	LV52-2-7a	Sandstone	this study
			LV52-2-7b	Sandstone	this study
			LV52-2-7v	Sandstone	this study
			LV52-2-7g	Sandstone	this study
			LV52-11-1	tuff diatomite	this study
LV52-11	44°29.45´ N 149°02.27´ E	2500–2200	LV52-11-2	tuff diatomite	this study
			LV52-11-3a	tuff sandstone	this study
			LV52-11-3v	Tuffite	this study
			LV52-11-3g	tuff diatomite	this study
			LV52-11-4	tuff diatomite	this study
LV52-12	44°28.618´ N 148°57.151´ E	2300–2000	LV52-12-1a	tuff diatomite	this study
			LV52-12-3	tuff diatomite	this study
LV52-13	44°28.129´ N 148°55.959´ E	2200–1900	LV52-13-4a	tuff diatomite	this study

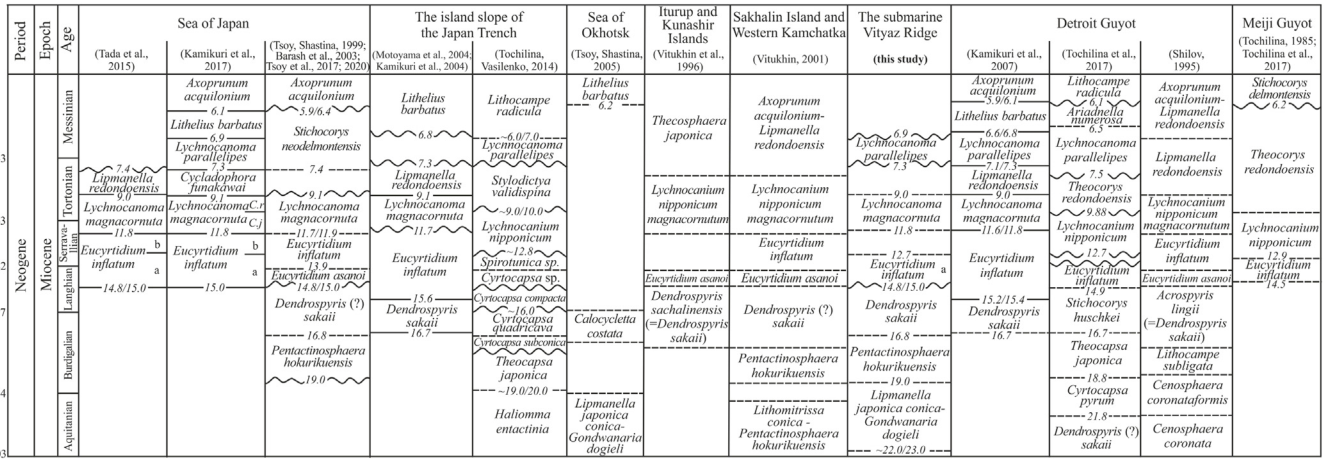

Fig. 2. Correlation between the Miocene radiolarian zones identified in the North Pacific and those on the SVR. Geological time scale ages are by Cohen et al. (2018). Radiolarian subzones abbreviations (Kamikuri et al., 2017): *C.r – Collosphaera reynoldsi, C.j – Cyrtocapsella japonica* (Barash et al., 2003).

the R/V *Akademik M. A. Lavrentyev* in 2005 and 2010, respectively. Brief lithological descriptions of the dredge samples are summarized in Table 1. According to previously published data (Lelikov et al., 2008; Terekhov et al., 2013), the SVR samples consist of slightly lithified sedimentary rocks represented by sandstone, tuffaceous diatomites, tuffaceous silty mudstones, tuffites, tuffs, and diatomaceous clay with ash. The bulk of the volcanogenic material is represented by explosive pyroclastics, which often contain fragments of quartz and pyroxene. The main mineral of rock cement is smectite. The samples from the southern part of the paraxial zone of the KKT contain grey diatomaceous clay with ash, including grains of quartz (Vasiliev, 1988).

Dredge samples are used because there are no other geological samples from this area. Although dredge samples cannot provide complete biostratigraphic information the quantitative data on radiolarian taxa abundances in the dredged samples can be used to identify radiolarian assemblages and correlate them with previously established zonal schemes in adjacent areas. To enhance the reliability of age results for the radiolarian assemblages in our samples, we incorporated biostratigraphic data for diatoms and silicoflagellates from the same samples (Terekhov et al., 2012, 2013; Tsoy, 2011, 2014; Tsoy, unpublished data).

3.2. Preparation

All stages of laboratory processing of samples and quantitative calculations are detailed in previous studies (Vasilenko and Vasilenko, 2021; Vasilenko, 2022). In summary, each bulk sediment sample was weighed and samples disaggregated by boiling in a 0.002 M solution of sodium pyrophosphate. Radiolarians were studied in the fraction > 40 μm using a LOMO Mikmed 6 Microscope (300 × magnification). We determined the total radiolarian content (TRC) (i.e., number of skeletons per gram of dry sediment), species richness (i.e., the number of species), and species relative abundances for each of the slides. The total radiolarian content were calculated as: TRC = $(n \times w_f)/(w_s \times w_p)$, where n is the number of skeletons on the slide; w_f is the weight of the > 40 μm fraction (g); w_s is the weight of the dry sediment (g); w_p is the weight the used aliquot of the > 40 μm fraction (g).

Radiolarian preservation was ranked as follows: poor, greater than 50 % of the skeletons were broken and/or exhibited signs of dissolution; moderate, 25–50 % of the skeletons were broken and/or exhibited signs of dissolution; and good, less than 25 % of the skeletons were broken and/or exhibited signs of dissolution.

The fossils were photographed under transmitted light using a Touptek photonics FMA050 digital camera. Additionally, the skeletal morphologies of the radiolarians were studied and photographed using a dual-beam scanning electron microscope (Tescan Lyra 3 XMH + EDS AZtec X-Max 80 Standart) at the micro- and nano-research laboratory of the Far Eastern Geological Institute FEB RAS (Vladivostok, Russia) and a scanning electron microscope (FEI Quanta 200 ESEM, FEI Company) at the First Oceanographic Institute of the Ministry of Natural Resources (Qingdao, China).

The applied taxonomic framework closely follows that of Tochilina (1996), Tochilina and Vasilenko (2018), and Afanasieva and Amon (2006).

3.3. Radiolarian zonation and datum levels

A few Neogene biostratigraphic schemes, with absolute age controls, have been developed for the northwestern part of the Pacific (Morley and Nigrini, 1995; Motoyama et al., 2004; Kamikuri et al., 2004, 2007, 2017; Tochilina et al., 2017) (Fig. 2). These schemes establish both the boundaries of chronostratigraphic units and the first (FO) and last occurrence (LO) of species, which are instrumental in determining the age of rocks, identifying the timing of global and regional geological events, and correlating these events. Since this investigation focuses on dredge samples, the age assigments for the FO and LO of radiolarian species are of utmost importance to determine the stratigraphic range of the studied deposits (Table 2).

Based on taxonomic composition and presence of zonal index species and characteristic species in the studied dredge samples, we identified Early–Late Miocene assemblage zones established in the northwestern Pacific. In this study, the radiolarian assemblage zones for the SVR and paraxial zone of the KKT were found to be consistent with those proposed by Reynolds (1980), Funayama (1988), Vitukhin (1993, 2001), Motoyama (1996), and Tsoy and Shastina (2005). We traced the assemblage zones, for which ages were established by Vitukhin (2001), Kamikuri et al. (2007, 2017), Tada et al. (2015), and Tsoy et al. (2020) (Fig. 2).

4. Results

In the studied dredge samples, we identified a total of 214 radiolarian species, including 105 species from 55 genera of Spumellaria, 107 species from 51 genera of Nassellaria, and 2 species from 1 genus of Collodaria. These findings allowed us to distinguish six radiolarian assemblages from the Early–Late Miocene (Fig. 3; Table S1).

Radiolarian assemblage I. The assemblage was observed in deposits on the southern plateau of the SVR (samples LV37-35-1, LV37-36-1, LV37-36-3, LV37-36-5, LV52-11-1, LV52-11-2, LV52-11-3a, LV52-11-3g, LV52-11-3v, and LV52-11-4). The TRC reaches 41,123 skeletons/g

Table 2
Radiolarian datum events (Ma) in the Northwest Pacific.

Species of Radiolaria	Sea of Japan (Site U1430)		Japan Trench (Site 1151)	Detroit Guyot (Site 884)	
	(Tada et al., 2015)	(Kamikuri et al., 2017)	Kamikuri et al., 2004)	(Morley, Nigrini, 1995)	(Kamikuri et al., 2007)
Lithelius barbatus		RI 6.8/7.0	RI 6.5/7.6		RI 6.6/6.8
Axoprunum acquilonium	LO 1.41	LO 1.7		LO 0.25	LO 0.3/0.4
	FO 7.1	FO 6.8–7.0	FO 6.5/7.6	FO 7.65	FO 6.6/6.8
Stichocorys delmontensis			LO 2.7/2.9	LO 6.45	LO 6.6/6.8
			ET 8.3/8.4		
Lychnocanoma parallelipes		LO 5.9/6.4	LO 5.9/6.0		LO5.9/6.1
		FO 7.2/7.4	FO 6.5/7.6		FO7.1/7.3
Lychnocanoma magnacornuta		LO 9.1	LO 8.6/9.2	LO 8.71	LO 7.1/7.3
	LCO 9.1	FO 11.7/11.9	LCO 8.6/9.2	FO 12.76	LCO 9.0
	FO 11.8		FO 11.7/14.2		FO 11.6/11.8
Cyrtocapsella tetrapera	RD 12.6	RD 12.8	RD 11.7/14.2		
Eucyrtidium inflatum	LO 11.8	LO 11.7/11.9	LO 14.2/14.6	LO 11.52	LO 11.6/11.8
			FO 15.2/15.3	FO 15.35	FO 15.2/15.4
Eucyrtidium asanoi		LO 13.8/14.1	LO 14.2/14.6	LO 13.52	LO 13.8/14.1
			FO 15.2/15.3	FO 16.24	FO 15.2/15.4
Dendrospyris sakaii	LO 14.8	LO 14.6/14.8	LO 14.8/14.9		LO 14.6/14.8
Pentactinosphaera hokurikuensis	LO 15.0		LO 14.9/15.1		LO 15.0/15.2

Note: FO = first occurrence, LO = last occurrence, LCO = last common occurrence, RD = rapid decrease, RI = rapid increase, ET = evolutionary transition.

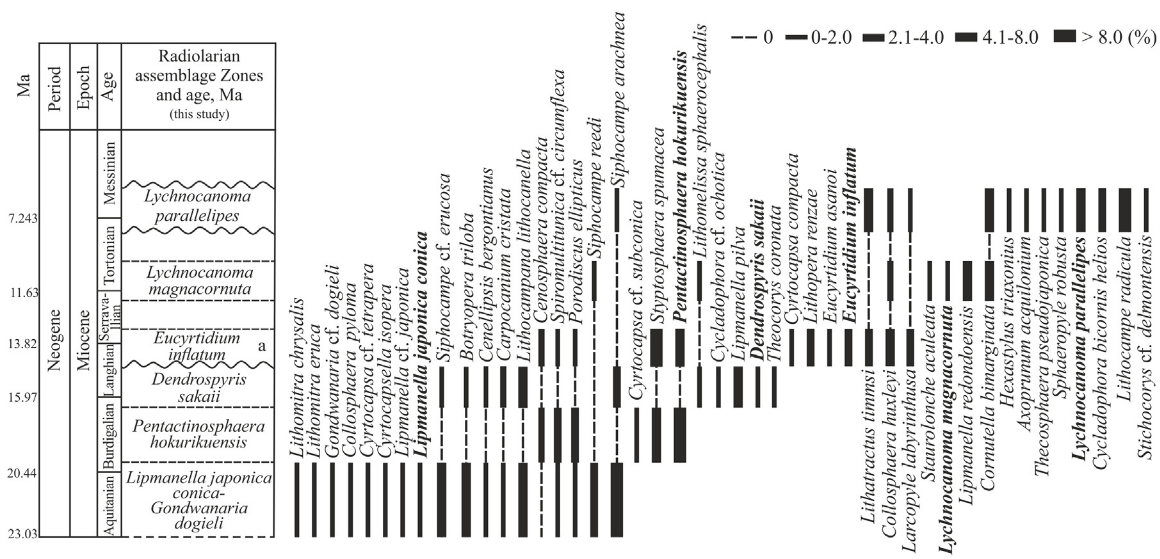

Fig. 3. Temporal changes in the relative abundance of selected radiolarian species in the studied deposits.

dry sediment, and preservation ranges from moderate to good. The assemblage is represented by a richness of 58–74 species (samples LV52-11-1 and LV52-11-4). From Table 3, one can see that there are about 6 samples where Spumellarians are dominant, and about 4 samples where Nassellarians are dominant, with the other samples displaying a more balanced split between these two categories. Oligocene species are present, including *Stylosphaera liostylus* Ehrenberg (up to 0.9 %), *Druppatractus polycentrus* Clark et Campbell (up to 2.2 %), *Prunopyle solida* Dreyer (up to 4.8 %), *Spirotunica* ex gr. *haackei* (Dreyer) (up to 1.0 %), *Spirotunica spiralis* (Dreyer) (up to 8.3 %), *Spongodiscus craticulatus* Stöhr (up to 1.6 %), *Sethopyramis quadrata* Haeckel (up to 1.9 %), and *Siphocampe* cf. *erucosa* Haeckel (up to 5.0 %). It also includes a large number of species from the Early Miocene, including *Cenellipsis bergontianus* Carnevale (up to 0.3 %), *Acanthosphaera castanea* Haeckel (up to 3.3 %), *Actinomma hootsi* (Campbell et Clark) (up to 4.1 %), *Haliometta miocenica* (Campbell et Clark) (up to 2.9 %), *Hexalonche octahedra* Haeckel (up to 1.9 %), *Larcopyle polyacantha amplissima* Lazarus, Faust et Popova (up to 1.2 %), *Spirotunica polyacantha* (Campbell et Clark) (up to 17.4 %), *Spongocore puer* Campbell et Clark (up to 4.5), *Carpocanium cristata* (Carnevale) (up to 0.3 %), *Cycladophora conica* Lombari et Lazarus (up to 2.9 %), *Cycladophora* ex gr. *golli* (Chen) Lombari et Lazarus (up to 1.3 %), *Lipmanella* cf. *japonica* (Nakaseko) (up to 0.3 %), *Lipmanella japonica conica* Petrushevskaya (up to 0.3 %), *Pseudodictyophimus* sp. F.2 (up to 1.9 %), *Lithomelissa tricornis* Chen (up to 0,3 %), *Gondwanaria dogieli* (Petrushevskaya) (up to 0.4 %), *Cyrtocapsella isopera* Chen (up to 3.7 %), *Siphocampe reedi* Campbell et Clark (up to 0.6), *Dendrospyris suganoi* Sugiyama et Furutani (up to 1.6 %), and *Botryopera triloba* (Ehrenberg) group (up to 44 %). One species of Collodaria occurs: *Collosphaera pyloma* Reynolds (up to 0.9 %) (Fig. 4).

The assemblage also contains species whose stratigraphic distribution spans a long interval of time, from the Oligocene to recent: *Pseudodictyophimus gracilipes* (Bailey) (up to 4.2 %), *Cyrtopera laguncula* Haeckel (up to 0.6 %), *Cornutella annulata* (Bailey) (up to 5.9 %), *Corocalyptra craspedota* (Jørgensen) (up to 3.5 %), *Ceratocyrtis* sp. (up to 1.6 %), and *Siphocampe arachnea* (Ehrenberg) (up to 26 %).

Sample LV37-36-1 contains two Late Miocene radiolarian species: *Theocalyptra bicornis spongothorax* Chen and *Spuroclathrocyclas parabicornis* (Hays) Tochilina et Vasilenko. These specimens were likely reworked. Most likely, the Lower Pliocene rocks were eroded into the Lower Miocene rocks, the outcrops of which are located lower on the

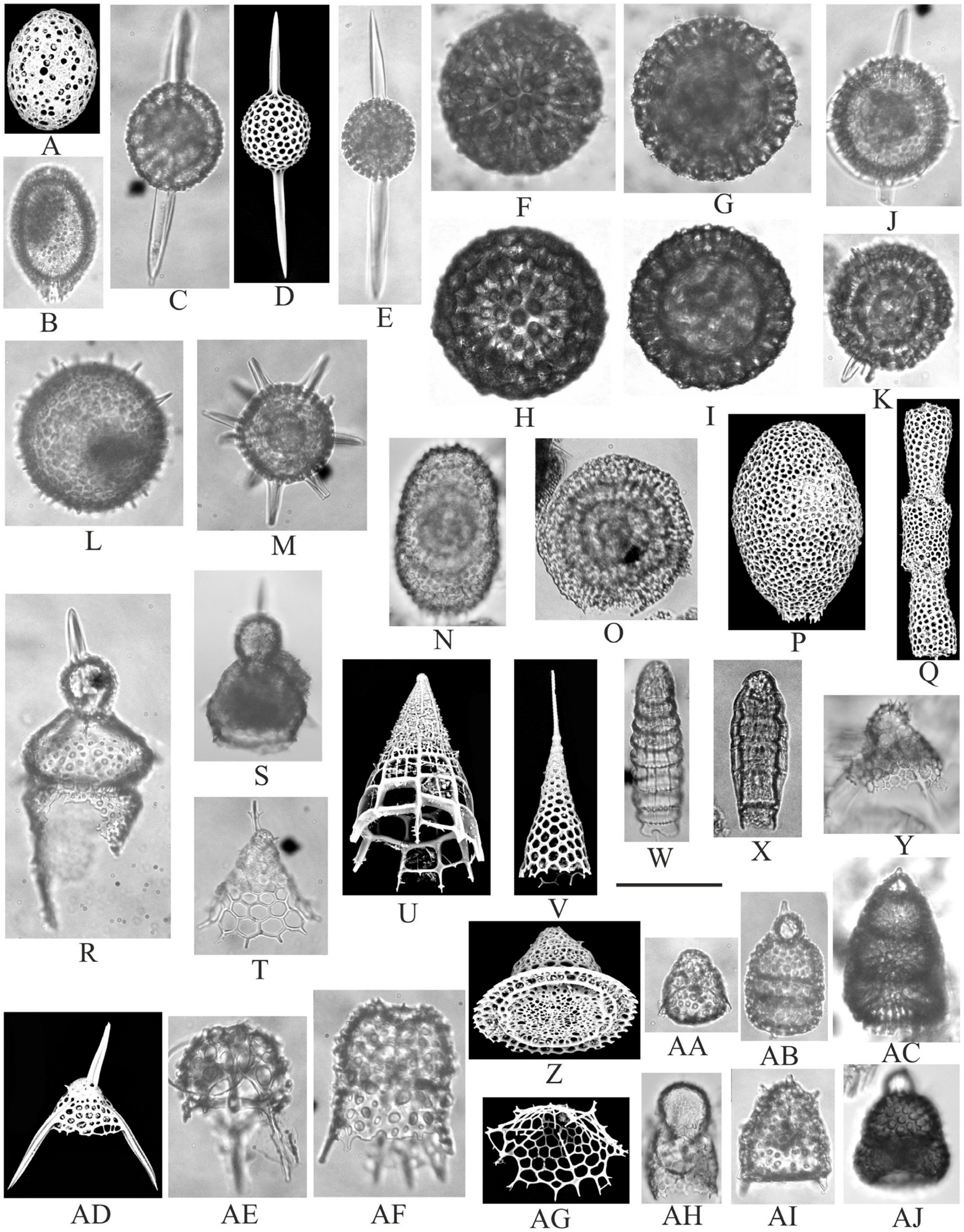

Fig. 4. Early Miocene radiolarians in the deposits from the SVR (*Lipmanella japonica conica-Gondwanaria dogieli* and *Pentactinosphaera hokurikuensis* assemblages). Scale bars = 100 μm. A. *Cenellipsis bergontianus* Carnevale, sample LV52-11-1. B. *Collosphaera pyloma* Reynolds, sample LV52-11-1. C. *Stylosphaera sulcata* Ehrenberg, sample LV52-11-1. D, E. *Druppatractus polycentrus* Clark et Campbell, sample LV52-11-1. E. F-I. *Pentactinosphaera hokurikuensis* (Nakaseko) F, G – (one specimen at various foci), sample 198-19, H, I – (one specimen at various foci), sample 198-5. J. *Stylosphaera angelina* Campbell et Clark, sample LV52-11-1. K. *Actinomma hootsi* (Campbell et Clark), sample LV52-11-1. L. *Acanthosphaera* cf. *castanea* Haeckel, sample LV52-11-1. M. *Haliometta miocenica* (Campbell et Clark), sample LV52-11-1. N. *Larcopyle polyacantha amplissima* Lazarus, Faust et Popova, sample LV52-11-4. O. *Ommatodiscus circularis* Carnevale, sample LV37-35-1. P. *Prunopyle titan* Campbell et Clark, sample LV52-11-1. Q. *Spongurus bilobatus* Clark et Campbell, sample LV52-11-1. R. *Lipmanella* cf. *japonica* (Nakaseko) *conica* Petrushevskaya, sample LV52-11-1. S. *Lipmanella japonica* (Nakaseko), sample LV52-11-3g. T. *Cycladophora conica* Lombari et Lazarus, sample LV52-11-1.U. *Plectopyramis dodecomma* Haeckel, sample LV52-11-1. V. *Cornutella orthoceras* (Haeckel), sample LV52-11-1. W. *Lithomitra eruca* Haeckel, sample LV52-11-1. X. *Siphocampe arachnea* (Ehrenberg), sample LV52-11-3g. Y. *Dictyophimus hertwigii* Haeckel, sample LV52-11-3v. Z. *Corocalyptra craspedota* (Jørgensen), sample LV52-11-1. AA. *Pseudodictyophimus* sp. F.1, sample LV52-11-3g. AB. *Cyrtocapsa* cf. *tetrapera* Haeckel, sample LV52-11-1. AC. *Cyrtocapsa* cf. *subconica* Nakaseko, sample 198–19. AD. *Pseudodictyophimus gracilipes* (Bailey), sample LV52-11-1. AE. *Dendrospyris* sp., sample LV52-11-1. AF. *Dendrospyris suganoi* Sugiyama et Furutani, sample LV52-11-1. AG. *Lampromitra* cf. *cachoni* Petrushevskaya, sample LV52-11-1. AH. *Botryopera triloba* (Ehrenberg), sample LV52-11-3v. AI. *Lithomelissa tricornis* Chen, sample LV52-11-1. AJ. *Theoconus* cf. *nipponicus* Nakaseko, sample LV37-35-1.

Table 3
Total radiolarian abundance (skeletons/g dry sediment) and quantitative analysis of radiolarian orders (%) in the studied dredge samples.

Radiolarian zones	Radiolarian assemblage	Dredge samples	Location	Total radiolarian content (skeletons/g)	The species richness (the number of taxa)	Spumellaria (%)	Nassellaria (%)	Collodaria (%)	Unidentified radiolarian (%)
Lychnocanoma parallelipes	VI	?LV52-2-7a	s.p	few	1	0	*	0	0
		?LV52-2-7b	s.p	few	1	*	0	0	0
		?LV52-2-7v	s.p	few	3	*	*	0	0
		?LV52-2-7g	s.p	few	3	*	*	0	0
		LV52-12-1a	s.p	2501	38	80.8	18.1	1.1	0
		N4-21/2-1	p.z. KKT	4099	28	52.5	34.3	0	13.2
		N4-21/2-2	p.z. KKT	10,738	43	38.9	58.4	0.7	2.0
Lychnocanoma magnacornuta	V	LV52-12-3	s.p	3124	36	43.7	52.7	3.6	0
Eucyrtidium inflatum a	IV	P-198-5	n.p	1368	38	85.3	11.8	1.9	1.0
		P-198-14	n.p	2098	21	80.4	11.2	5.6	2.8
Dendrospyris sakaii	III	LV52-13-4a	s.p	10,678	42	27.3	61.9	1.4	9.4
Pentactinosphaera hokurikuensis	II	P-198-19	n.p	1200	17	96.6	3.4	0	0
Lipmanella japonica conica-Gondwanaria dogieli	I	LV52-11-2	s.p	few	5	*	0	0	0
		LV52-11-3a	s.p	2049	11	41.7	41.7	0	16.6
		LV52-11-3v	s.p	5241	25	28.0	59.0	0	13.0
		LV52-11-3g	s.p	41,123	44	20.5	73.9	0	5.6
		LV52-11-4	s.p	1776	58	44.0	45.3	0	10.7
		LV52-11-1	s.p	9294	74	50.6	43.7	0.6	5.1
		LV37-35-1	s.p	6294	22	74.8	19.9	0	5.3
		LV37-36-1	s.p	314	15	70.3	29.7	0	0
		LV37-36-3	s.p	few	5	*	*	0	0
		LV37-36-5	s.p	3617	30	45.4	51.0	2.7	0.9

Note:
* Presence of sporadic radiolarian taxa. Location of the dredge samples: s.p: southern plateau of the SVR, n.p: northern plateau of the SVR, and p.z. KKT: the paraxial zone of the KKT.

slope of the Bussol Strait. This is indicated by the better preservation of Early Miocene radiolarian skeletons, while the Early Pliocene radiolarian skeletons are either satisfactory or poor.

Radiolarian assemblage II. The assemblage was observed in deposits on the northern plateau of the SVR (sample 198–19). The TRC was 1,200 skeletons/g dry sediment, and the skeletal preservation was good. The assemblage includes 17 species, most of which were Spumellaria (96.6 %) (Table 3). These specimens mainly have spherical shapes: *Cenosphaera compacta* Haeckel (up to 3.4 %), *Styptosphaera spumacea* Haeckel (up to 7.0 %), *Actinomma sexaculeatum* (Stöhr) (up to 3.4 %). *Pentactinosphaera hokurikuensis* (Nakaseko) (up to 20.8%) dominated. The assemblage also includes species with a spiral skeletal structure, such as *Lithelius nautiloides* Popofsky (up to 7.0 %), *Spirotunica irregularis* (Dreyer) (up to 3.4 %), *Spirotunica polyacantha* (Campbell et Clark) (up to 3.4 %), *Porodiscus ellipticus* Carnevale (up to 3.4 %), as well as some with spongy skeletal structure, including *Spongurus pylomaticus* Riedel (up to 3.4 %), *Spongodiscus resurgens* Ehrenberg (up to 7.0 %), *Stylotrochus sol* Campbell et Clark (up to 3.4 %). Nassellaria are represented by a single but stratigraphically important species: *Cyrtocapsa* cf. *subconica* Nakaseko (up to 3.4 %) (Fig. 4). Many of the species in Assemblage II (*Styptosphaera spumacea, Lithelius nautiloides, Porodiscus ellipticus, Spongurus pylomaticus, Spongodiscus resurgens, Stylotrochus sol*) also live in the modern ocean.

Radiolarian assemblage III. The assemblage was observed in deposits on the southern plateau of the SVR (sample LV52-13-4a). The TRC is 10,680 skeletons/g dry sediment, and the skeletal preservation is moderate to good (Table 3). The assemblage is characterized by Polycystinea radiolarians and included 42 species. Collodaria are also present with 1.4 % abundance. Nassellaria (61.9 %) predominate slightly; however, a pronounced dominance of any genera or species is not observed in the assemblage. The species in this assemblage include: *Druppatractus irregularis* Popofsky (2.6 %), *Actinomma echinoideum* Carnevale (1.4 %), *Larcopyle* cf. *nebulum* Lazarus, Faust et Popova (1.4 %), *Stylodictya stellata* Bailey (1.4 %), *Spongodiscus* ex gr. *gigas* Campbell et Clark (1.4 %), *Cycladophora* cf. *ochotica* Vitukchin (1.4 %), *Theocorys* cf. *coronata* (Carnevale) (1.4 %), *Lipmanella pilva* Vitukhin (4.1 %), *Lithomelissa sphaerocephalis* Chen (1.4 %), *Lithostrobus nucula* Ehrenberg (2.6 %), *Lithobotrus* sp. (1.4 %), and *Dendrospyris sakaii* Sugiyama et Furutani (1.4 %) (Fig. 5).

Radiolarian assemblage IV. The assemblage was observed in deposits on the northern plateau of the SVR (samples 198-5 and 198-14). The assemblage includes Polycystinea and Collodaria specimens. The TRC is 1,368–2,098 skeletons/g dry sediment, and the skeletal preservation is good. The observed specimens belong to 21–38 species (Table 3), with dominance of Spumellaria (80.4–85.3 %). The assemblage includes the following Spumellaria species: *Styptosphaera spumacea* Haeckel (4.0–11.1 %), *Stylosphaera angelina* Campbell et Clark (7.7–8.2 %), *Lithatractus timmsi* Campbell et Clark (up to 2.8 %), *Thecosphaera concentrica* Nakaseko (1.0–5.6 %), *Thecosphaera japonica* Nakaseko (up to 5.6 %), *Pentactinosphaera hokurikuensis* (Nakaseko) (2.8–5.8 %), *Carposphaera magnaporulosa* Clark et Campbell (up to 6.8 %), *Spiromultitunica* cf. *circumflexa* Tochilina et Popova (up to 3.4 %), *Larcopyle labyrinthusa* Lazarus, Faust et Popova (up to 2.8 %), *Spirotunica polyacantha* (Campbell et Clark) (6.8–8.2 %), and *Stylodictya tenuispina* Jørgensen (up to 1.0 %) (Fig. 5). Nassellaria, which are not numerous, are represented by the following species: *Eucyrtidium inflatum* Kling (1.9–2.8 %), *Eucyrtidium asanoi* Sakai (up to 1.0 %), *Lipmanella* sp. (1.0–5.6 %), *Cyrtocapsa compacta* Haeckel (up to 1.0 %), and *Lithopera renzae* Sanfilippo et Riedel (up to 2.8 %). Collodaria are represented by one species: *Collosphaera huxleyi* Müller (1.9–5.6 %). The assemblage also contains poorly preserved radiolarians with similar morphological features as *Stichomitra, Diacanthocapsa*, and *Stichocapsa*. The poor skeletal preservation indicated that these specimens were reworked.

Radiolarian assemblage V. The assemblage was observed in deposits from the southern plateau of the SVR (sample LV52-12-3). The assemblage includes Polycystinea and Collodaria specimens. The TRC is 3,124 skeletons/g dry sediment, and the skeletal preservation is good. The specimens belong to 36 species (Table 3), and Nassellaria (52.7 %) dominate slightly. Collodaria are represented by one species: *Collosphaera huxleyi* Müller (3.6 %). The species are representative of a wide age range, such as in the assemblages described below, including *Carposphaera magnaporulosa* Clark et Campbell (1.8 %), *Lithe-*

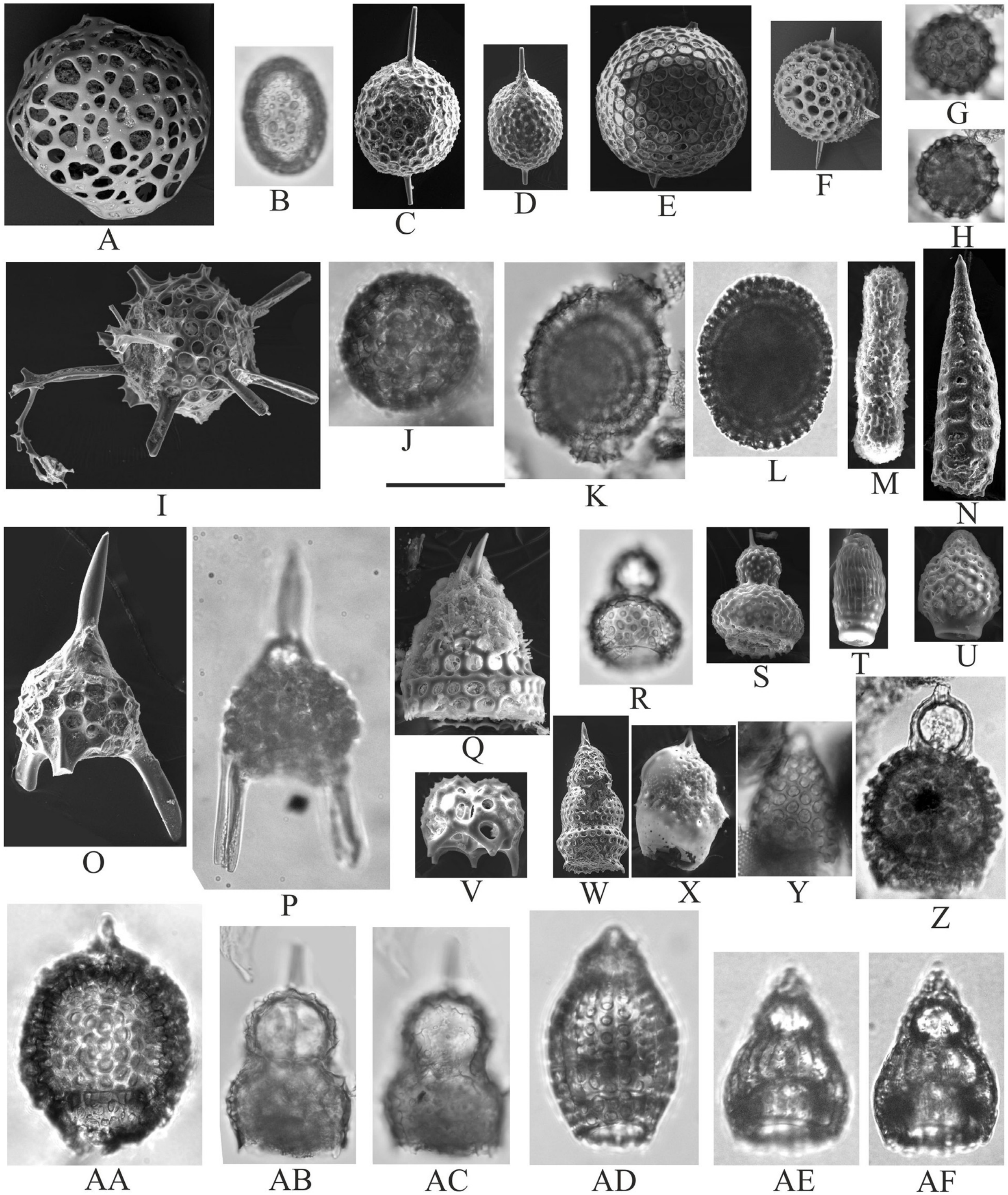

Fig. 5. Middle–Late Miocene radiolarians in the deposits from the SVR (*Dendrospyris* (?) *sakaii, Eucyrtidium inflatum,* and *Lychnocanoma magnacornuta* assemblages). Scale bars = 100 μm. A. *Collosphaera hüxleyi* Müller, sample LV52-12-3. B. *Cenellipsis bergontianus* Carnevale, sample LV52-13-4a. C. *Stylosphaera* cf. *gonioxyphos* Clark et Campbell, sample LV52-12-3. D. *Druppatractus* sp., sample LV52-12-3. E. *Hexacontium* sp., sample LV52-12-3. F. *Staurolonche* cf. *aculeata* Campbell et Clark, sample LV52-12-3. G, H. *Carposphaera magnaporulosa* Clark et Campbell (one specimen at various foci), sample LV52-13-4a. I. *Cladococcus* cf. *stalactites* Haeckel, sample LV52-12-3. J. *Styptosphaera spumacea* Haeckel, sample 198–14. K. *Lithelius* sp., sample LV52-13-4a. L. *Spiromultitunica* cf. *circumflexa* Tochilina et Popova, sample 198–5. M. *Spongocore puer* Campbell et Clark, sample LV52-13-4a. N. *Cornutella bimarginata* Haeckel, sample LV52-12-3. O, P. *Lychnocanoma magnacornuta* Sakai, sample LV52-12-3. Q. *Cycladophora* cf. *ochotica* Vitukhin, sample LV52-13-4a. R, S. *Lipmanella pilva* Vitukhin, sample LV52-13-4a. T. *Lithomitra lineata* Ehrenberg, sample LV52-13-4a. U. *Carpocanium cristata* (Carnevale), sample LV52-13-4a. V. *Dendrospyris sakaii* Sugiyama et Furutani, sample LV52-13-4a. W. *Lithostrobus cornutus* Haeckel, sample LV52-12-3. X. *Lithobotrus* sp., sample LV52-13-4a. Y. *Lithocampana lithocanella* Clark et Campbell, sample LV52-13-4a. Z. *Lipmanella redondoensis* (Campbell et Clark), sample LV52-12-3. AA. *Lithopera renzae* Sanfilippo and Riedel, sample 198–14. AB, AC *Lithomelissa sphaerocephalis* Chen (one specimen at various foci), sample LV52-13-4a. AD. *Eucyrtidium inflatum* Sakai, sample 198–5. AE, AF. *Eucyrtidium asanoi* Sakai (one specimen at various foci), sample 198–5.

lius minor Jørgensen (3.6 %), *Spirotunica polyacantha* (Campbell et Clark) (3.6 %), *Stylodictya validispina* Jørgensen (1.8 %), *Stylodictya stellata* Bailey (1.8 %), *Cycladophora* ex gr. *golli* Lombari et Lazarus (1.8 %), *Cycladophora conica* Lombari et Lazarus (3.6 %), *Lithomelissa sphaerocephalis* Chen (1.8 %), *Pseudodictyophimus gracilipes* (Bailey) (1.8 %), *Cyrtopera laguncula* Haeckel (3.6 %), *Lithostrobus cornutus* Haeckel (1.8 %), and *Siphocampe reedi* Campbell et Clark (1.8 %). In addition, the sample includes species not found in older assemblages, such as *Druppatractus* sp. (3.6 %), *Cladococcus* cf. *stalactites* Haeckel (1.8 %), *Haliomma* cf. *medusa* Ehrenberg (3.6 %), *Staurolonche* cf. *aculeata* Campbell et Clark (1.8 %), *Spongopyle setosa* Dreyer (1.8 %), *Cornutella bimarginata* Haeckel (5.5 %), *Lipmanella redondoensis* (Campbell et Clark) (7.3 %), *Lychnocanoma magnacornuta* Sakai (1.8 %), and *Ceratospyris* sp. (7.3 %) (Fig. 5).

Radiolarian assemblage VI. The assemblage was observed in deposits from the southern plateau of the SVR and the paraxial zone of the KKT (samples LV52-2-7a-1, LV52-2-7b, LV52-2-7g, LV52-2-7v, LV52-12-1a, N4-21/2-1, and N4-21/2-2). The assemblage includes Polycystinea and Collodaria specimens. The TRC is highly variable and ranges from single specimens on the southern plateau of the SVR to 10,738 skeletons/g dry sediment in the paraxial zone of the KKT. The skeletal preservation is poor to good. Spumellaria (80.8 %) dominate in the southern plateau of the SVR (sample LV52-12-1), whereas no dominance is observed in the paraxial zone of the KKT. Species richness is also variable, with 1–38 species on the southern plateau of the SVR and 28–43 species in the paraxial zone of the KKT (Table 3). Common species for both areas include *Collosphaera huxleyi* Müller (up to 1.1 %), *Actinomma echinoideum* Carnevale (up to 14.6 %), *Larnacalpis* sp. (up to 1.1 %), *Stylodictya stellata* Bailey (up to 4.5 %), *Lithocampe radicula* Ehrenberg (up to 19.6 %), and *Stichocorys delmontensis* Campbell et Clark (up to 1.5 %). Other species in these areas differ. The assemblage of the southern plateau SVR includes: *Amphisphaera cristata* Carnevale (up to 1.1 %), *Amphisphaera* cf. *spinosa* Carnevale (up to 2.1 %), *Xiphatractus brevispina* Carnevale (up to 1.1 %), *Xiphatractus santaeannae* (Campbell et Clark) (up to 2.1 %), *Hexacontium subtile* Carnevale (up to 8.4 %), *Hexalonche aristarchi* Haeckel (up to 1.1 %), *Hexastylus* ex gr. *spiralis* Haeckel (up to 1.1 %), *Hexastylus triaxonius* Haeckel (up to 1.1 %), *Heliodiscus asteriscus* Haeckel (up to 1.1 %), *Spirema melonia* Haeckel (up to 1.1 %), *Larcopyle weddellium* Lazarus, Faust et Popova (up to 3.2 %), *Lithelius nautiloides* Popofsky (5.3 %), *Lychnocanoma parallelipes* Motoyama (3.2 %), *Cycladophora bicornis helios* Lombari et Lazarus (up to 2.1 %), *Anthocyrtris ehrenbergi* Stöhr (up to 2.1 %), *Ceratocyrtis stoermeri* Goll et Bjørklund (up to 1.1 %), and *Cyrtocapsa meta* (Stöhr) (up to 1.1 %). The assemblage of the paraxial zone of the KKT includes: *Axoprunum acquilonium* (Hays) (up to 1.5 %), *Thecosphaera pseudojaponica* Nakaseko (up to 2.0 %), *Tholospyra cervicornis* Haeckel (up to 7.5 %), *Cornutella hexagona* Haeckel (up to 2.6 %), *Lithocampe platycephala* (Ehrenberg) (up to 0.7 %), *Botryostrobus bramlettei* (Campbell et Clark) (up to 3.0 %), *Eucyrtidium acuminatum* Ehrenberg (up to 0.7 %), *Eucyrtidium punctatum* Ehrenberg (up to 0.7 %), *Botryocampe inflata* (Bailey) (up to 0.7 %), and *Petalospyris foveolata* Ehrenberg (up to 0.7 %) (Fig. 6).

Such a difference in the observed generic and species composition of radiolarians is explained by the difference in sampling locations and depths (Table 1).

This assemblage also included two Late Miocene species, namely, *Theocalyptra bicornis spongothorax* Chen (Fig. 6) and *Spuroclathrocyclas parabicornis* (Hays) Tochilina et Vasilenko.

5. Discussion

5.1. Miocene biostratigraphy of the submarine Vityaz Ridge

We correlated the six radiolarian assemblages recognized in this study with previously established radiolarian assemblage zones for the northwestern Pacific and adjacent seas. During this process, we based these correlations on the presence of index species of the corresponding zones, the ages of FO and LO index species (Table 2), and similarities in the taxonomic composition. As a result, the sequence of the radiolarian zones can be considered as the Miocene biostratigraphic scheme for the SVR.

***Lipmanella japonica conica-Gondwanaria dogieli* Zone** (Tsoy and Shastina, 2005; emended by the present study)

Definition: This zone was defined as the interval from the FO of *Lipmanella japonica conica* Petrushevskaya (base) to the FO of *Pentactinosphaera hokurikuensis* (Nakaseko) (top).

Faunal characteristics: The assemblage zone includes the zonal index species *Lipmanella japonica conica* Petrushevskaya and *Gondwanaria dogieli* (Petrushevskaya) (species richness and diversity are given in Section 4, Radiolarian assemblage I, and Table S1).

Correlation and age: At the beginning of the Early Miocene, dramatic changes occurred in the diversity of radiolarians. Most Oligocene species disappeared and many new species appeared, which then became widespread in the Miocene. These "new" species included *Lipmanella japonica conica* Petrushevskaya. The species characterize the Early Miocene *Velicucullus oddgurneri–Lipmanella japonica conica* assemblage of the Norwegian Sea (Strelkov and Petrushevskaya, 1979). Bjørklund (1976) recognized the *Lipmanella* (= *Gondwanaria*) *japonica* Zone in the Lower Miocene sediments of this sea (Bjørklund, 1976). In turn, Petrushevskaya (Strelkov and Petrushevskaya, 1979) attributed the lower part of this zone to the *Velicucullus oddgurneri–Lipmanella japonica conica* assemblage, and established that the typical *Lipmanella japonica* (Nakaseko) is absent in the lower parts of layers belonging to the *Velicucullus oddgurneri–Lipmanella japonica conica* assemblage. Instead of *Lipmanella japonica* (Nakaseko), these layers contain the subspecies *Lipmanella japonica conica* Petrushevskaya. Thus, the age of *Velicucullus oddgurneri–Lipmanella japonica conica* assemblage corresponds to the beginning of the Early Miocene (Strelkov and Petrushevskaya, 1979).

Tsoy and Shastina (2005) studied radiolarian and diatom assemblages in dredge samples from the submarine Terpeniya Ridge (Sea of Okhotsk). They found the index species *Lipmanella japonica conica* Petrushevskaya and typical species *Gondwanaria dogieli* (Petrushevskaya) of the *Velicucullus oddgurneri–Lipmanella japonica conica* assemblage from the Norwegian Sea. Based on this, Tsoy and Shastina (2005) established the *Lipmanella japonica conica–Gondwanaria dogieli* assemblage for the submarine Terpeniya Ridge and traced the assemblage to the northern slope of the Kuril Basin. They determined that the age of this assemblage is the end of the Late Oligocene to the beginning of the Early Miocene.

Based on the presence of index species and species from the genera *Spongodiscus, Pseudodictyophimus, Lithocampana, Lipmanella, Lithomitra*, we trace the *Lipmanella japonica conica–Gondwanaria dogieli* assemblage in the sediments of the SVR. A feature of the assemblage in the SVR sediments is the single presence of the index species *Lipmanella japonica conica* Petrushevskaya and *Gondwanaria dogieli* (Petrushevskaya), which contrasts with their high content in sediments of the Sea of Okhotsk. Based on the taxonomic composition of this assemblage from the SVR being similar to that of the *Velicucullus oddgurneri–Lipmanella japonica conica* assemblage, we consider that the age of the *Lipmanella japonica conica–Gondwanaria dogieli* assemblage is the beginning of the Early Miocene.

In the samples studied here, the radiolarian *Lipmanella japonica conica–Gondwanaria dogieli* assemblage occurs within the diatom *Thalassiosira praefraga* Zone (24.0–20.3 Ma) and silicoflagellate *Naviculopsis lata* Zone (Tsoy, 2011; 2014) (Fig. 7). The top boundary of the diatom *Thalassiosira praefraga* Zone is close to the base boundary of the radiolarian *Pentactinosphaera hokurikuensis* Zone. Considering all of the above, the *Lipmanella japonica conica–Gondwanaria dogieli* assemblage can probably be defined as a zone using the same name and with the corresponding boundaries. Accordingly, we propose that the base of

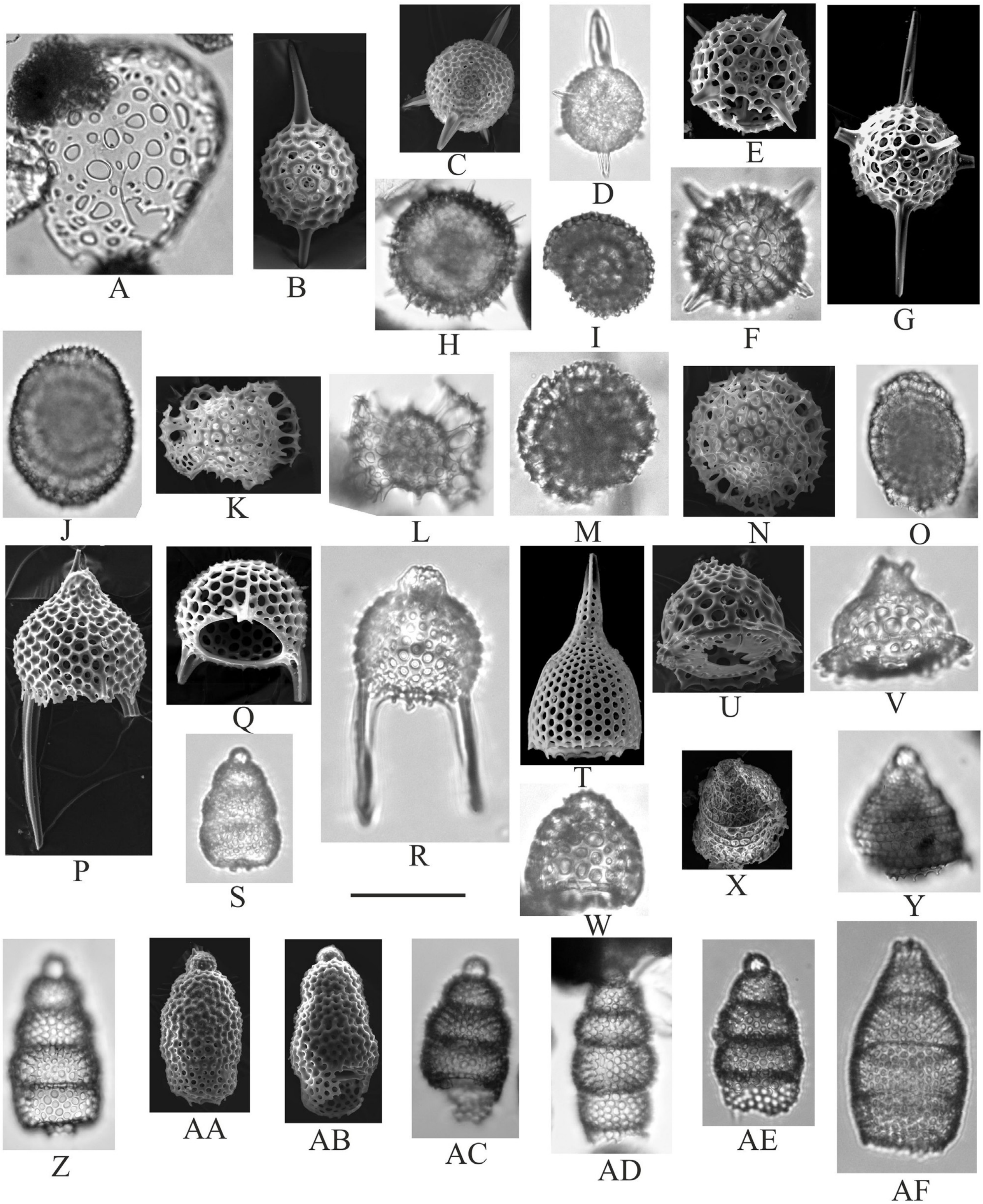

Fig. 6. Last Miocene radiolarians in the deposits from the SVR (*Lychnocanoma parallelipes* assemblage). Scale bars = 100 μm. A. *Collosphaera hüxleyi* Müller, sample LV52-12-1. B. *Xiphatractus santaeannae* (Campbell et Clark), sample LV52-12-1a. C, D. *Amphisphaera* cf. *spinosa* Carnevale, sample LV52-12-1a. E, F. *Hexalonche aristarchi* Haeckel, sample LV52-12-1a. G. *Hexastylus* ex gr. *spiralis* Haeckel, sample LV52-12-1a. H. *Actinomma echinoideum* Carnevale, sample LV52-12-1a. I. *Spirema melonia* Haeckel, sample LV52-12-1a. J. *Spirotunica irregularis* (Dreyer), sample LV52-12-1a. K, L. *Larnacalpis* sp., sample LV52-12-1a. M, N. *Lithelius nautiloides* Popofsky, sample LV52-12-1a. O. *Larcopyle weddellium* Lazarus, Faust et Popova, sample LV52-12-1a. P-R. *Lychnocanoma parallelipes* Motoyama group., sample LV52-12-1a. S. *Cyrtocapsa* cf. *meta* (Stöhr), sample LV52-12-1a. T. *Anthocyrtris ehrenbergi* Stöhr, sample LV52-12-1a. U, V. *Cycladophora bicornis helios* Lombari et Lazarus, sample LV52-12-1a. W. *Ceratocyrtis stoermeri* Goll et Bjørklund, sample LV52-12-1a. X, Y. *Theocalyptra bicornis spongothorax* Chen, sample LV37-36-1. Z-AE. *Lithocampe radicula* Ehrenberg group., Z-AD – sample LV52-12-1a, AE – sample N4-21/2-2. AF. *Eucyrtidium acuminatum* Ehrenberg, sample N4-21/2-2.

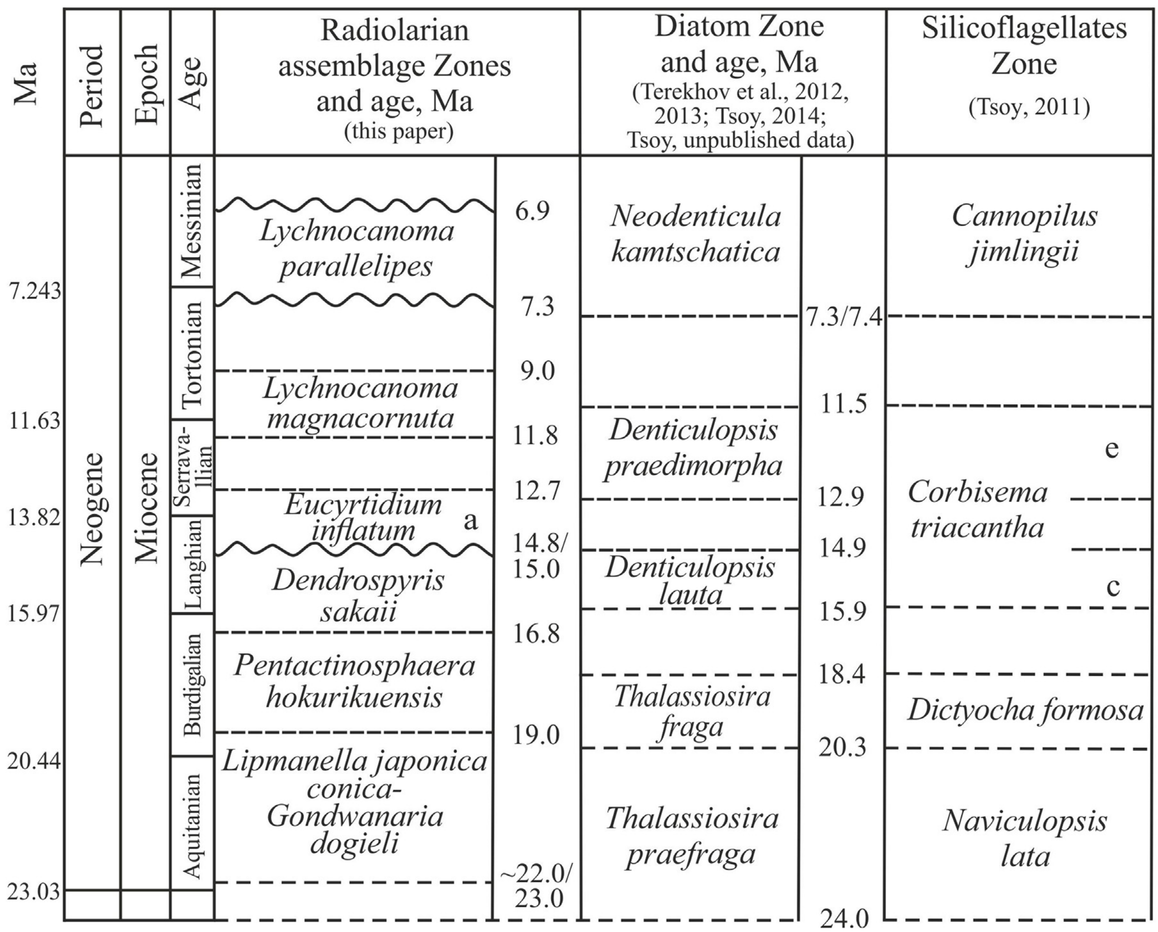

Fig. 7. Correlation between the Miocene radiolarian zones and diatom and silicoflagellate zones identified in the deposits from the SVR.

the *Lipmanella japonica conica–Gondwanaria dogieli* Zone approximately coincides with the Oligocene–Miocene boundary at 22.0/23.0 Ma and the top of the zone corresponds to the base of the overlying *Pentactinosphaera hokurikuensis* Zone at 19 Ma (Fig. 7).

***Pentactinosphaera hokurikuensis* Zone** (Vitukhin, 1993, 2001)

Definition: The zone is defined as the interval from the FO of *Pentactinosphaera hokurikuensis* (Nakaseko) (base) to the FO of *Dendrospyris sakaii* Sugiyama et Furutani (top). The acme of *Pentactinosphaera hokurikuensis* (Nakaseko) is observed within the zone (Vitukhin, 2001).

Faunal characteristics: The assemblage of this zone includes the zonal index species *Pentactinosphaera hokurikuensis* (Nakaseko) at up to 20.8 % (species richness and diversity are given in Section 4, Radiolarian assemblage II, and Table S1).

Correlation and age: Vitukhin (1993) identified the *Pentactinosphaera hokurikuensis* Zone in the Pestrotsvetnaya Formation on Karaginsky Island (Eastern Kamchatka). Later, Shilov (1995) identified the *Cenosphaera coronataformis* Zone in the Lower Miocene sediments of the Detroit Guyot (ODP, Hole 884B) (Fig. 2). Vitukhin (1999) established the identity of the index species *Pentactinosphaera hokurikuensis* (Nakaseko) and *Cenosphaera coronataformis* Shilov and the corresponding zones.

Motoyama et al. (2010) found that the assemblage of this zone has common elements with the Kamenoo and Taira Formation groups in the Joban area (Japan) and the Isshi Formation group in Mie Prefecture (Japan). They also traced the *Pentactinosphaera hokurikuensis* Zone in the Kushiro submarine canyon (the continental slope of eastern Hokkaido) and proposed that its age is 19.0–17.5 Ma.

We consider that the age of the base boundary of the *Pentactinosphaera hokurikuensis* Zone is 19.0 Ma, in accordance with Motoyama et al. (2010). The age of the top boundary corresponds to the basal age of the *Dendrospyris sakaii* Zone at 16.8 Ma according to Tada et al. (2015). In the samples here studied, the radiolarian *Pentactinosphaera hokurikuensis* Zone is occurring within the diatom *Thalassiosira fraga* Zone (20.3–18.4 Ma) and the silicoflagellate *Dictyocha formosa* Zone (Tsoy, 2011, 2014) (Fig. 7).

***Dendrospyris sakaii* Zone** (Vitukhin, 1993, 1999)

Definition: The zone is defined as the interval from the FO of *Dendrospyris sakaii* Sugiyama et Furutani (base) to the FO of *Eucyrtidium asanoi* Sakai (top) (Shilov, 1995 emend. Vitukhin, 1999, 2001).

Faunal characteristics: The assemblage of this zone includes the zonal index species *Dendrospyris sakaii* Sugiyama et Furutani (species richness and diversity are given in Section 4, Radiolarian assemblage III, and Table S1).

Correlation and age: The *Dendrospyris sakaii* Zone (= *Dendrospyris sachalinensis* (Vitukhin, 1993) = *Acrospyris lingii* (Shilov, 1995)) was first identified in the upper part of the Pil'skaya Formation of the Machigar section of the Schmidt Peninsula (Northern Sakhalin) (Vitukhin, 1993). This zone correlates with the Middle Miocene diatom *Denticulopsis praelauta* Zone (16.3–15.9 Ma) and *Denticulopsis lauta* Zone (15.9–14.9 Ma) (Vitukhin, 1993). Kamikuri et al. (2004) established the location of the Early–Middle Miocene boundary within the *Dendrospyris sakaii* Zone (IODP, Hole 1151A). According to the results of deep-sea drilling in the Sea of Japan, the age of the *Dendrospyris sakaii* Zone is 16.8–14.8 Ma (Tada et al., 2015). Later, using the same samples, Kamikuri et al. (2017) established the age of the base of the *Eucyrtidium inflatum* Zone as 15 Ma (Fig. 2). The *Eucyrtidium inflatum* Zone overlies the *Dendrospyris sakaii* Zone. In line with the results of Tada et al. (2015) and Kamikuri et al. (2017), the age of the top boundary of the *Dendrospyris sakaii* Zone is 14.8/15 Ma.

We consider that the age of the *Dendrospyris sakaii* Zone is 16.8–14.8/15.0 Ma, following Tada et al. (2015) and Kamikuri et al. (2017). In the samples studied here, the radiolarian *Dendrospyris sakaii* Zone occurs within the diatom *Denticulopsis lauta* Zone (15.9–14.9 Ma) and the lower part of the silicoflagellate *Corbisema triacantha* c Subzone (Tsoy, 2012; Terekhov et al., 2013) (Fig. 7).

***Eucyrtidium inflatum* Zone, Subzone a** (Reynolds, 1980, emended by Funayama, 1988)

Definition: The subzone is defined as the interval from the FO of *Eucyrtidium inflatum* Sakai (base) to the rapid decrease (RD) of *Cyrtocapsella tetrapera* Haeckel (top) (Funayama, 1988).

Faunal characteristics: This interval includes the zonal index species *Eucyrtidium inflatum* Kling (species richness and diversity are given in Section 4, Radiolarian assemblage IV, and Table S1).

Correlation and age: The *Eucyrtidium inflatum* Zone was identified by Reynolds (1980) within Middle Miocene sediments of the island slope of the Japan Trench. Funayama (1988) divided it into two subzones “a” and “b”. According to the results of deep-sea drilling in the Sea of Japan, the age of the subzone “a” is 15.0–12.7 Ma and that of the subzone “b” is 12.7–11.8 Ma (Kamikuri et al., 2017). The assemblage of subzone “a” includes *Pentactinosphaera hokurikuensis* (Nakaseko) (LO–15.0 Ma) and *Eucyrtidium asanoi* Sakai (LO–14.1/13.8 Ma), and the assemblage of subzone “b” contains the FO of *Lychnocanoma magnacornuta* Sakai (11.7–11.9 Ma) (Kamikuri et al., 2017).

Radiolarian assemblage IV contains *Pentactinosphaera hokurikuensis* (Nakaseko) and *Eucyrtidium asanoi* Sakai. In the same samples, single specimens of the diatom zonal index species *Denticulopsis lauta* (Bailey) Simonsen were found (Tsoy, unpublished data). The age of the *Denticulopsis lauta* Zone is 15.9–14.9 Ma (Barron and Gladenkov, 1995; Gladenkov, 2007). In turn, LO *Denticulopsis lauta* (Bailey) Simonsen was recorded near the base of the diatom *Crucidenticula nicobarica* Zone (13.1–12.9 Ma) (Barron and Gladenkov, 1995; Gladenkov, 2007). This allows us to confidently assign the radiolarian assemblage IV to the lower part of subzone “a”.

We consider that the age of the Subzone a of the *Eucyrtidium inflatum* Zone is 14.8/15.0–12.7 Ma, which is according to Tada et al. (2015) and Kamikuri at al. (2017) (Fig. 7).

***Lychnocanoma magnacornuta* Zone** (Funayama, 1988)

Definition: The zone is defined as the interval from the FO (base) to LCO (top) of *Lychnocanoma magnacornuta* Sakai by Motoyama (1996).

Faunal characteristics: This interval includes the zonal index species *Lychnocanoma magnacornuta* Sakai (species richness and diversity are given in Section 4, Radiolarian assemblage V, and Table S1).

Correlation and age: The *Lychnocanoma magnacornuta* Zone was identified by Funayama (1988) in the Middle–Upper Miocene deposits of the Noto Peninsula (Japan). Vitukhin et al. (1996) traced the assemblage of the *Lychnocanoma magnacornuta* Zone in marine sections of the Kuibyshevskaya Formation of Iturup Island and Lovtsovskaya Formation of Kunashir Island (Greater Kuril Ridge).

We consider that the age of the *Lychnocanoma magnacornuta* Zone is 11.8–9.0 Ma, according to Tada et al. (2015) and Kamikuri et al. (2017). In the samples here studied, the radiolarian *Lychnocanoma magnacornuta* Zone occurs within the diatom *Denticulopsis praedimorpha* Zone (12.9–11.5 Ma) and the top part of the silicoflagellate Subzone e of the *Corbisema triacantha* Zone (Tsoy, 2012; Terekhov et al., 2013) (Fig. 7).

***Lychnocanoma parallelipes* Zone** (Motoyama, 1996)

Definition: The zone is defined as the interval from the FO of *Lychnocanoma parallelipes* Motoyama (base) to the rapid increase (RI) of *Lithelius barbatus* Motoyama (top) (Motoyama, 1996).

Faunal characteristics: This interval includes the zonal index species *Lychnocanoma parallelipes* Motoyama (species richness and diversity are given in Section 4, Radiolarian assemblage VI, and Table S1).

Correlation and age: The *Lychnocanoma parallelipes* Zone was identified by Motoyama (1996) in the Sea of Japan. Later, Kamikuri et al. (2017) determined that the age of the zone is 7.3–6.9 Ma (Fig. 2).

The radiolarian assemblage VI contains index species of the *Lychnocanoma parallelipes* Zone, *Axoprunum acquilonium* Zone, *Lithocampe radicula* Zone, and *Stichocorys delmontensis* Zone (Fig. 2). Nevertheless, we correlate this assemblage with the *Lychnocanoma parallelipes* Zone since these species are present, as accessory species, in the faunal composition of this zone. Moreover, in the same samples, Tsoy (unpublished data) established the diatom *Neodenticula kamtschatica* Zone. The age of the diatom zone is 7.3/7.4–3.9/4.0 Ma (Barron and Gladenkov, 1995; Gladenkov, 2007). This confirms our choice of the *Lychnocanoma parallelipes* Zone for the correlation of radiolarian assemblage VI.

We consider that the age of the *Lychnocanoma parallelipes* Zone is 7.3–6.9 Ma, according to Kamikuri et al. (2017). As previously noted, in the samples we studied, the radiolarian *Lychnocanoma parallelipes* Zone is occurring within the diatom *Neodenticula kamtschatica* and the silicoflagellate *Cannopilus jimlingiie* Zone (Tsoy, unpublished data) (Fig. 7).

5.2. Paleoceanography of the SVR during the Miocene

At the beginning of the Early Miocene (~22.0/23.0–19.0 Ma), radiolarian assemblages from the southern plateau of the SVR (in this study) are close to those of the Terpeniya Ridge (southwest of the Sea of Okhotsk) and the Kuril Basin (Tsoy and Shastina, 2005). Tsoy and Shastina (2005) indicate that during this period, sedimentation in the southern part of the Sea of Okhotsk occurred under conditions of transgression, resulting in a wide connection between the sea and the Pacific Ocean. The similarity of radiolarian assemblages allows us to assume deep-sea sedimentation conditions also in the area of the southern plateau of the SVR. This assumption is confirmed by previously obtained data on the existence of bathyal conditions in the area at this time (Terekhov et al., 2012, 2013; Tsoy, 2014).

At the end of the Early Miocene (19.0–16.8 Ma) and in the Middle Miocene (14.8/15.0–12.7 Ma), *Pentactinosphaera hokurikuensis* (Nakaseko) dominated radiolarian assemblages in the area of the northern plateau of the SVR. We believe that this species is typical of shallow water and possibly coastal habitats. This assumption is supported by the fact that *Pentactinosphaera hokurikuensis* (Nakaseko) is characteristic of the earliest stage of the opening of the Sea of Japan and characterizes the transition from freshwater to marine conditions (Ling, 1992; Tsoy et al., 2017, 2020). The association of this species with sediments accumulated during the transition from freshwater to marine conditions is confirmed by Miyamoto et al. (2022). They discovered a *Pentactinosphaera-Cyrtocapsella* (P-C) assemblage consisting of *Pentactinosphaera hokurikuensis* (Nakaseko) and *Cyrtocapsella tetrapera* (Haeckel) in the sedimentary layers of Oki Dogo Island (southwest Japan) immediately overlying nonmarine sediments. Based on the study of mid-Miocene diatom assemblages, Tsoy and Shastina (2005) also suggested that the northern plateau of the SVR formed under upper bathyal conditions with active removal of sediments from nearby coastal areas.

During the Middle Miocene, erosion of pre-Cenozoic sediments occurred on the northern plateau of the SVR, as evidenced by the presence of poorly preserved Cretaceous species in the radiolarian assemblage. These taxa were redeposited from bedrock of the northern plateau or introduced from pre-Cenozoic sediments of the Kamchatka Peninsula, where similar taxa were identified by Palechek et al. (2005).

In addition, the Middle Miocene radiolarian assemblage of the northern plateau of the SVR includes the warm-water species *Lithopera renzae* Sanfilippo and Riedel and *Collosphaera huxleyi* Müller. The presence of these warm-water species suggests that the area was influenced by warm-water masses during the Middle Miocene. Vitukhin (1993) discovered warm-water radiolarian species in the Middle Miocene Formation of the Plosky Cape (Karaginsky Island, Eastern Kamchatka) and attributed their presence to the influence of warm-water masses and climate warming in the northern Pacific. The regional warming of the environment discovered by our group and Vitukhin (1993) represents an expression of the first Miocene climatic optimum at the end of the Early to beginning of the Middle Miocene (Gladenkov, 1982, 1988; Gladenkov, 1998; Zachos et al., 2001). At this time, marine southern boreal shallow-water assemblages (with subtropical species) were spreading far to the north of Kamchatka and Alaska (Gladenkov, 1998).

In the Late Miocene (11.6/11.8–9.0 Ma), the radiolarian assemblage of the southern plateau SVR included warm-water species *Collosphaera huxleyi* Müller, *Cladococcus* cf. *stalactites* Haeckel, and *Lithostrobus cornutus* Haeckel. These species are characteristic of the water masses of the Sea of Japan and the island slope of the Japan Trench. Runeva and Ushko (1984) also found warm-water Collodaria in Upper Miocene marine sections of the Kunashir Island and Iturup Island (Greater Kuril Chain). The presence of these taxa indicates the influence of warm water masses on the study area during the beginning of the Late Miocene. This influence temporally coincides with the second Miocene climatic optimum, which was recorded in the northern part of the Pacific for different groups of fossil communities of fauna and flora (Gladenkov, 1982, 1988).

At the end of the Late Miocene (7.1/7.3–6.6/6.8 Ma), the sediments of the near-axial zone of the KKT (opposite the Bussol Strait) also contain warm-water species *Collosphaera huxleyi* Müller and *Heliodiscus asteriscus* Haeckel. The presence of these warm-water species suggests that the area continued to be influenced by warm water masses at the end of the Late Miocene.

In the area of the Bussol Strait, a mixture of Early Miocene and Late Miocene–Early Pliocene radiolarian species is observed. The source of Late Miocene species for this mixed assemblage is probably the Upper Miocene–Lower Pliocene sequence recognized in the sediments of the Bussol Strait (Vasiliev et al., 1979). The presence of this radiolarian assemblage indicates the activation of erosion processes at the end of the Late Miocene–Early Pliocene in the area of the Bussol Strait. Erosion of sediments in the Late Miocene–Early Pliocene has also been established for the region of the northern plateau of the SVR (Terekhov et al., 2012).

6. Conclusions

In the sediments of the SVR and paraxial zone of the KKT, Miocene radiolarian faunas were identified, including 105 species from 55 genera of Spumellaria, 107 species from 51 genera of Nassellaria, and 2 species from 1 genus of Collodaria. The highest TRC (41,123 skeletons/g dry sediment) and richest species composition (74 species) were observed in the Early Miocene.

The biostratigraphy was established based on radiolarian assemblages from dredge samples, and a sequence of assemblages (*Lipmanella japonica conica–Gondwanaria dogieli, Pentactinosphaera hokurikuensis, Dendrospyris sakaii, Eucyrtidium inflatum* Subzone a, *Lychnocanoma magnacornuta* and *Lychnocanoma parallelipes*) was determined. The age of the zones was determined based on correlations with deep-sea drilling data in the Sea of Japan, the island slope of the Japan Trench, and the Detroit Guyot. As a result, we constructed a biostratigraphic scheme for radiolarians from the Miocene in the SVR.

Our study contributes to the history of the geological and environmental development of the SVR in the Miocene. In particular, we showed that at the beginning of the Early Miocene, sedimentation occurred on the southern plateau of the SVR under bathyal conditions; at the end of the Early Miocene, sedimentation occurred on the northern plateau of the SVR under shallow water conditions. In the Middle and Upper Miocene sediments of the southern SVR plateau and Middle Miocene sediments of the northern plateau of the SVR, we recognized two Miocene climatic optima that were previously established in the North Pacific.

A continuation of our work in other geological intervals will make it possible to reconstruct the history of the geological development of the SVR in the Cenozoic. However, many questions about the geological history of the region can only be resolved after deep-sea drilling.

Declaration of competing interest

There are no conflicts of interest to declare.

Data availability

Data will be made available on request.

Funding

This study was funded by the Ministry of Sciences and Education of the Russian Federation (project number 124022100084-8) and the Science and Technology Innovation Project of Laoshan Laboratory (project number LSKJ202204203).

Acknowledgements

We would like to express our sincere gratitude to Dr. R.G. Kulinich and Dr. M.G. Valitov for providing the dredge samples. We also thank the anonymous reviewers for their comments and suggestions for improving the article.

Supplementary materials

Supplementary material associated with this article can be found, in the online version, at doi:10.1016/j.revmic.2024.100789.

References

Afanasieva, M.S., Amon, E.O., 2006. Radiolarians 320.
Barash, M.S., Kazarina, G.Kh., Kruglikova, S.B., Safarova, S.A., Khankishieva, L.M., 2003. On the Neogene paleogeography of the North Yamato Rise (Sea of Japan) from biostratigraphic and seismostratigraphic data. Oceanology 43 (4), 542–550.
Barron, J.A., Gladenkov, A.Y., 1995. Early Miocene to Pleistocene diatom stratigraphy of Leg 145. Proc. ODP, Sci. Results 145, 3–19 (Ocean Drilling Program 145.
Bjørklund, K.R., 1976. In: Radiolaria from the Norwegian Sea, Leg 38 of the Deep Sea Drilling Project //Initial Reports of the Deep Sea Drilling Project. Wash, 38. U.S. Government Printing Office, pp. 1101–1168.
Cohen, K.M., Finney, S.C., Gibbard, P.L., Fan, J.X., 2018. The ICS International Chronostratigraphic Chart. Episode 36, 199–204.
Funayama, M., 1988. Miocene radiolarian stratigraphy of the Suzu area, northeastern part of the Noto Peninsula, Japan. Contrib. Inst. Geol. Paleontol. Tohoku Univ. 91, 15–41.
Gladenkov, Yu.B., 1982. Neogene climatic fluctuations in northern Kamchatka. Doklady of the academy of sciences of the USSR. Earth Sci. Sect. 265 (2), 407–409.
Gladenkov, Yu.B., 1988. In: Marine Neogenes Stratigraphy of the Northern Part of the Pacific belt (Review of the Stratigraphical Schemes For the Far East of the USSR, North America and Japan, 428. Nauka, Moscow, p. 212 in Russian.
Gladenkov, A.Yu., 1998. Oligocene and lower Miocene diatom zonation in the North Pacific stratigraphy and geological correlation 6 (2), 50–64.
Gladenkov, A.Yu., 2007. Late Cenozoic Detailed Stratigraphy and Marine Ecosystems of the North Pacific Region (based on Diatoms). GEOS, Moscow, p. 296.
Hays, J.D., 1970. Stratigraphy and evolutionary trends of Radiolaria in North Pacific Deep-Sea Sediments. Geol. Soc. Am. Mem. Memoir 126, 185–218. doi:10.1130/MEM126-p185.
Kamikuri, S., Nishi, H., Motoyama, I., Saito, S., 2004. Middle Miocene to Pleistocene radiolarian biostratigraphy in the Northwest Pacific Ocean, Ocean Drilling Program, Leg 186. Isl. Arc. 13, 191–226. doi:10.1111/j.1440-1738.2003.00421.x.
Kamikuri, S., Nishi, H., Motoyama, I., 2007. Effects of late Neogene climatic cooling on North Pacific radiolarian assemblages and oceanographic conditions. Palaeogeogr. Palaeoclimatol. Palaeoecol. 249, 370–392. doi:10.1016/j.palaeo.2007.02.008.
Kamikuri, S., Itaki, T., Motoyama, I., Matsuzaki, K.M., 2017. Radiolarian biostratigraphy from middle Miocene to late Pleistocene in the Japan Sea. Palaeontol. Res. 21, 397–421. doi:10.2517/2017PR001.
Khomich, V.G., Boriskinaa, N.G., Kasatkin, S.A., 2019. Geology, magmatism, metallogeny, and geodynamics of the South Kuril Islands. Ore Geol. Rev. 105, 151–162. doi:10.1016/j.oregeorev.2018.12.015.

Kozlova, G.E., Gorbovets, A.N., 1966. Radiolarians of the Upper Cretaceous and Upper Eocene Deposits of the West Siberian Lowland, 158. Nedra, Leningrad in Russian.

Kulinich, R.G., Karp, B.Y., Baranov, B.V., Lelikov, E.P., Karnaukh, V.N., Valitov, M.G., Nikolaev, S.M., Kolpashchnikova, T.N., Tsoy, I.B., 2007. Structural and Geological Characteristics of a "Seismic Gap" in the Central Part of the Kuril Island Arc. Russ. J. Pac. Geol. 1 (1), 3–14. doi:10.1134/S1819714007010022.

Kulinich, R.G., Valitov, M.G., Proshkina, Z.N., 2015. Comparative analysis of seismic and density models of the Earth's crust of the Central Kuril Islands. Russ. J. Pac. Geol. 9 (6), 439–450. doi:10.1134/S1819714015060068.

Lelikov, E.P., Tsoy, I.B., Emel'yanova, T.A., Terekhov, E.P., Vashchenkova, N.G., Vagina, N.K., Smirnova, O.L., Khudik, V.D., 2008. Geological structure of the submarine Vityaz Ridge within the Seismic Gap area (Pacific slope of the Kurile Island Arc). Russ. J. Pac. Geol. 2 (2), 99–109. doi:10.1134/S1819714008020012.

Leonteva, V.V., 1985. Hydrology of the Trenches of the World Ocean, 208. Nauka, Moscow in Russian.

Ling, H.Yi., 1992. Radiolarians from the Sea of Japan: leg 128. In: Proc. ODP, Sci. Results, 127/128, 127/128. Ocean Drilling Program, College Station, TX, pp. 225–236.

Lipman, R.X., Burtman, E.C., Khokhlova, I.A., 1960. Stratigraphy and fauna of the Paleogene deposits of the West Siberian Lowland. Proceedings of VSEGEI: VSEGEI, Nov. Series. Issue, 28. 231. (in Russian).

Miyamoto, H., Hayashi, H., Itaki, T., 2022. Radiolarian biostratigraphy of the Miocene Kumi Formation in Oki Dogo Island, Southwest Japan. J. Geol. Soc. Jpn. 128 (1) 377–3.

Morley, J.J., Nigrini, C., 1995. Miocene to Pleistocene radiolarian biostratigraphy of North Pacific sites 881, 884, 885, 886 and 887. In: Proc. Ocean Drill. Program, 145. Texas A&M University, Sci. Results, pp. 55–91.

Motoyama, I., 1996. Late Neogene radiolarian biostratigraphy in the subarctic Northwest Pacific. Micropaleontology 42 (3), 221–262.

Motoyama, I., Niitsuma, N., Maruyama, T., Hayashi, H., Kamikuri, S., Shiono, M., Kanamatsu, T., Aoki, K., Morishita, C., Hagino, K., Nishi, H., Oda, M., 2004. Middle Miocene to Pleistocene magneto-biostratigraphy of ODP Sites 1150 and 1151, northwest Pacific: sedimentation rate and updated regional geological timescale. Isl. Arc. 13, 289–305. doi:10.1111/j.1440-1738.2003.00426.x.

Motoyama, I., Kamikuri, S., TuZino, T., Kawamura, K., Miwa, T., 2010. Radiolarians from rock samples recovered from the Kuroshio submarine canyon. Bull. Geol. Surv. Japan 61, 87–103. doi:10.9795/bullgsj.61.87.

Nakaseko, K., Sugano, K., 1973. Neogene radiolarian zonation in Japan. Geol. Soc. Jpn, Mem. 8, 23–34.

Palechek, T.N., Baraboshkin, E.J., Solovjev, A.V., Lopatina, D.A., Lander, A.V., 2005. New Data on a Structure and Age Mesozoic and Cenozoic deposits of Cape Hajryuzova (Western Kamchatka). Western Kamchatka: Geological Development in Mesozoic. Institute of the Lithosphere, Marginal and Inner Seas, Geological Institute of Russian Academy of Science. Publishing house the Nauchnyi Mir, Moscow, pp. 77–91 in Russian.

Popova, I.M., 1989. Some Aspects of Paleooceanological Studies of the Paleogene-Neogene basins of South Sakhalin and Eastern Kamchatka. Paleontological and Stratigraphic Studies of the Phanerozoic of the Far East Russia. FESC AS USSR, Vladivostok, pp. 63–68.

Reynolds, R.A., 1980. Radiolarians from the western North Pacific, Leg 57, Deep Sea Drilling Project. In: Scientific Party, Initial Reports of the Deep Sea Drilling Project, 56–57. U. S. Government Printing Office, Washington, DC, pp. 735–769.

Runeva, N.P., 1981. Radiolarians from the Reference Sections of the Cenozoic of Southern Sakhalin and Western Kamchatka. Systematics, Evolution and Stratigraphic Significance of Radiolarians. Nauka, Moscow, pp. 91–95 in Russian.

Runeva, N.P., Ushko, K.A., 1984. Neogene Radiolarians of the Great Kuril Ridge and Their Stratigraphic Significance. Microfauna of Oil and Gas Regions of the USSR. VNIGRI, Leningrad, pp. 94–101 in Russian.

Sergeev, K.F., 1976. Tectonic of Kuril island System, 239. Nauka, Moscow in Russian.

Shilov, V.V., 1995. Miocene-Pliocene radiolarians from Leg 145, North Pacific. In: Proc. Ocean Drill. Program. Sci. Results, 145. Texas A&M University, pp. 93–116.

Strelkov, A.A., Petrushevskaya, M.G., 1979. Exploration of the Fauna of the Seas. The history of the Microplankton of the Norwegian Sea (on the Deep Sea Drilling materials). Nauka. Academy of Sciences of the USSR, Zoological Institute, Leningrad, USSR.

Tada, R., Murray, R.W., Alvarez Zarikian, C.A., et al., 2015. In: Proc. Integrated Ocean Drilling Program, 346. Integrated Ocean Drilling Program, College Station, TX, pp. 1–113. doi:10.2204/iodp.proc.346.110.2015.

Terekhov, E.P., Mozherovsky, A.V., Tsoy, I.B., Lelikov, E.P., Vashchenkova, N.G., Gorovaya, M.T., 2012. Late Mesozoic and Cenozoic volcano sedimentary complexes from the submarine Vityaz Ridge, the Island Arc slope of the Kuril-Kamchatka Trench, and its evolution. Russ. J. Pac. Geol. 6, 209–216. doi:10.1134/S1819714012030062.

Terekhov, E.P., Tsoy, I.B., Mozherovsky, A.V., Lelikov, E.P., Vashchenkova, N.G., Vagina, N.K., Gorovaya, M.T., Smirnova, O.L., 2013. Stratigraphy of the submarine Vityaz Ridge (External arc of the Kuril island-arc system). Oceanological Studies of the Far-Eastern seas and Northwestern Pacific 2, 111–119 in Russian.

Tochilina, S.V., 1985. Biostratigraphy of the Cenozoic of the Northwestern Pacific. Nauka, Moscow, p. 134 in Russian.

Tochilina, S.V., 1991. The Oligocene – Miocene boundary at the juncture of the Japan and Kuril Island arcs. Fifth International Congress on Pacific Neogene stratigraphy and IGCP-246, Japan, 114–115.

Tochilina, S.V., 1996. On the Problem of the Systematics of Nassellaria (Radiolaria). Biochemical peculiarities. Evolution. FEB RAS, Vladivostok, p. 51.

Tochilina, S.V., 2013. On the problem of boundaries in the Neogene. Oceanological studies of the Far Eastern seas and the northwestern part of the Pacific Ocean. In two books. Vladivostok. Dal'nauka 2, 170–176 in Russian.

Tochilina, S.V., Goll, I.M., Vasilenko, L.N., Mozherovsky, A.V., 2017. The features of the geological structure of the northern part of the Emperor Ridge (deep sea drilling sites at the Detroit and Meiji Guyots) (Pacific Ocean). Russ. J. Pac. Geol. 36 (5), 92–115.

Tochilina, S.V., Vasilenko, L.N., 2018. Atlas of Cenozoic Radiolarians from the Northwest Pacific. POI FEB RAS, Vladivostok, p. 128.

Tsoy, I.B., 2002. Oligocene diatom assemblages from the island slope deposits of the Kuril-Kamchatka Trench. Oceanology 42 (2), 252–265.

Tsoy, I.B., 2011. Silicoflagellates of the Oligocene–Early Miocene submarine Vityaz Ridge (Island Slope of the Kurile–Kamchatka Trench). Algologiya 1, 111–125 in Russian.

Tsoy, I.B., 2012. Zonal complexes of diatoms and silicoflagellates from Cenozoic deposits of the submarine Vityaz Ridge (island slope of the Kuril-Kamchatka Trench). In: Proceedings of the LVIII session of the Paleontological Society at the Russian Academy of Sciences. Paleontology and stratigraphic boundaries (St. Petersburg, April 2-6, 2012). VSEGEI, St. Petersburg, pp. 153–154 in Russian.

Tsoy, I.B., 2014. Upper Oligocene–Lower Miocene diatom assemblages of the submarine Vityaz Ridge (island slope of the Kuril-Kamchatka Trench). Stratigr. Geol. Correl. 22 (6), 618–631. doi:10.1134/S0869593814060069.

Tsoy, I.B., Shastina, V.V., Gorovaya, M.T., 2000. Micropaleontological Characteristics of the Cenozoic deposits of the Kronotsky Bay (Eastern Kamchatka), 23. POI FEB RAS, Vladivostok in Russian.

Tsoy, I.B., Shastina, V.V., 2005. Cenozoic Siliceous Microplankton from the Sediments of the Sea of Okhotsk and Kurile–Kamchatka Trench, 181. Dal'nauka, Vladivostok in Russian.

Tsoy, I.B., Gorovaya, M.T., Vasilenko, L.N., Vashchenkova, N.G., Vagina, N.K., 2017. Age and conditions of formation of sedimentary cover of the Ulleung Plateau of the Sea of Japan according to micropaleontological data. Stratigr. Geol. Correl. 25 (1), 99–121. doi:10.1134/SO8695938170100063.

Tsoy, I.B., Vashchenkova, N.G., Vasilenko, L.N., Gorovaya, M.T., Vagina, N.K., Melnichenko, Yu.I., 2020. Age and Formation conditions of Cenozoic sedimentary cover of the Yamato Rise in the Sea of Japan. Stratigr. Geol. Correl. 28 (2), 202–229. doi:10.1134/S0869593820020069.

Udintsev, G.B., 1955. Relief of the Kuril-Kamchatka Depression. In: Proceedings of the Institute of Science of the USSR Academy of Sciences. Research of the Kuril-Kamchatka Depression, 12. Publishing House of the Academy of Sciences of the USSR, Moskow, Leningrad, pp. 12–61 in Russian.

Vasilenko, L.N., 2017. Oligocene-Early Miocene radiolarians from the sediments of southern plateau of the submarine Vityaz Ridge (island slope of the Kuril–Kamchatka Trench) and their stratigraphic value. Bulletin of Kamchatka Regional Association, Educational-Scientific Center. Earth Sci. 35 (3), 87–102 in Russian.

Vasilenko, L.N., 2022. Radiolarian data from the submarine Vityaz Ridge, Northwest Pacific, for biostratigraphic and paleoceanographic reconstructions. Data Brief 42, 108092. doi:10.1016/j.dib.2022.108092.

Vasilenko, L.N., Vasilenko, Yu.P., 2021. Pleistocene radiolarian biostratigraphy of the submarine Vityaz Ridge, Northwest Pacific. Mar. Micropaleontol. 169, 102040. doi:10.1016/j.marmicro.2021.102040.

Vasiliev, B.I., 1988. Main Features of the Geological Structure of the Northwestern Pacific. FEB of USSR Academy of Sciences, Vladivostok, p. 192 in Russian.

Vasiliev, B.I., Zhiltsov, E.G., Suvorov, A.A., 1979. The Geological Structure of the Southwestern Part of the Kuril arc–Trench System, 106. Nauka, Moskow in Russian.

Vasiliev, B.I., Sigova, K.L., Objirov, A.I., Yugov, I.V., 2001. Geology and Oil-Gas Resources of the Marginal Seas of the Northwestern Pacific. Dal'nauka, Vladivostok, p. 309 in Russian.

Vitukhin, D.I., 1989. Radiolarian complexes from Neogene deposits of the Kuril Islands (Kunashir, Iturup). Cenozoic of the Far East Russia. Vladivostok, 206–208. (in Russian).

Vitukhin, D.I., 1993. Separation of the Cenozoic of the Far East Russia by Radiolarians, 104. Nauka, Moscow in Russian.

Vitukhin, D.I., 1999. Radiolaria. In: Cenozoic Ecosystems of the Okhotsk Sea region. The Paleogene and Neogene Key Section of North Sakhalin (Shmidt Peninsula): stratigraphy, paleogeography, and Geological Events. GEOS, Moskow, pp. 61–65.

Vitukhin, D.I., 2001. Zonal Radiolarian Scales of the Cenozoic of the Boreal Pacific and Its Northwestern Framing (history, Current state, and problems). Ways to Detail Stratigraphic Schemes and Paleogeographic Reconstructions. GEOS, Moscow, pp. 159–168 in Russian.

Vitukhin, D.I., Oreshkina, T.V., Pushcharovskiy, Yu.M., Tsukanov, N.V., 1996. New data on the geology of Iturup Island (Kuril Island Arc). Stratigr. Geol. Correl. 4 (6), 61–74.

Worne, S., Kender, S., Swann, G.E.A., Leng, M.J., Ravelo, A.C., 2019. Coupled climate and subarctic Pacific nutrient upwelling over the last 850,000 years. Earth Planet. Sci. Lett. 522, 87–97. doi:10.1016/j.epsl.2019.06.028.

Zachos, J.C., Shackleton, N.J., Revenaugh, J.S., et al., 2001. Climate response to orbital forcing across the Oligocene-Miocene boundary. Science 292 (5515), 274–278.